HELLENIC REPUBLIC
National and Kapodistrian University of Athens

"ALEXANDER FLEMING"
Biomedical Sciences Research Center

MSc in Molecular Biomedicine:

''Mechanisms of Disease, Molecular and Cell Therapies and Bio-innovation''

Master Thesis Dissertation

Monogiou Eirini-Anastasia

Project Title:

'' Functional characterization of novel DNA Damage Response (DDR) genes ''

Committee

Dr. Fousteri Maria	**Dr Panayotou George**	**Dr Kotsinas Athanassios**
Researcher B'	Researcher A'	Assistant Professor
BSRC ''Alexander Fleming''	BSRC ''Alexander Fleming''	National Kapodistrian University of Athens
		Medical School

Vari, 24 July 2019

Acknowledgements

First of all, I would like to thank my supervisor, Dr. Fousteri Maria, for giving me the opportunity to be a member of her research group as well as for the guidance & support throughout my Master Thesis project. Besides my advisor, I would like to thank the rest of my thesis committee: Dr Panayotou George and Prof Kotsinas Athanassios.

I would also like to express my gratitude to Dr. Eszter Szantai for our pleasant and effective collaboration, the continuous support, the patience and help throughout my study. My sincere thanks go to Dr Stefos Georgios and the rest lab members for creating a great work environment.

Table of Contents

Abstract

Our cells have evolved to deal with thousands of DNA damage events that occur every day, activating the DNA Damage Response (DDR) network. **DDR** is a complex mechanism that leads to cell-cycle arrest, regulation of DNA replication, repair or bypass of DNA damage. UV irradiation is a damaging agent that leads to bulky adducts, distorting the structure of the double helix and Nucleotide Excision Repair **(NER**) is the mechanism that orchestrate the repair of the UV-induced lesions. The research team of Dr Fousteri has developed the **aniFOUND method** for the isolation and study of the chromatin that is repaired and newly synthesized via NER. Coupling of aniFOUND with mass spectrometry analysis resulted in a list of proteins indicating an involvement in UV-DDR network. In this study, we characterized a number of the newly isolated factors. For this purpose, small interfering RNAs (siRNAs) and lentiviral short hairpin RNAs (shRNAs) gene silencing strategies were chosen to knock down the DDR candidate proteins. In addition, wild type fibroblasts were UV-C irradiated and immunofluorescence analysis was performed to verify their recruitment at local UV damage sites (LUDs) providing insights into their implication in the UV-DDR network.

Keywords: *DNA damage response (DDR), Nucleotide Excision Repair (NER), UV irradiation, LUDs, siRNAs, shRNAs, gene silencing*

Περίληψη

Χιλιάδες βλάβες λαμβάνουν χώρα στο γενετικό μας υλικό κάθε μέρα και τα κύτταρα μας έχουν εξελιχθεί ώστε να τις αντιμετωπίζουν, ενεργοποιώντας το μηχανισμό απόκρισης στις βλάβες του DNA (DNA Damage Response-DDR). Αυτός ο πολύπλοκος μηχανισμός, μπορεί να οδηγήσει στη διακοπή του κυτταρικού κύκλου, στη ρύθμιση της αντιγραφής του DNA, την επισκευή ή και την παράκαμψη της βλάβης του DNA. Η υπεριώδης UV ακτινοβολία είναι ένας εξωγενής επιβλαβής παράγοντας, ο οποίος οδηγεί στην προσθήκη ογκωδών μορίων, παραμορφώνοντας τη δομή της διπλής έλικας του DNA. Η επιδιόρθωση των επαγόμενων βλαβών από την υπεριώδη ακτινοβολία ενορχηστρώνεται από τον μηχανισμό εκτομής νουκλεοτιδίων (Nucleotide Excision Repair -NER). Η ερευνητική ομάδα της Δρ. Φουστέρη έχει αναπτύξει τη μέθοδο aniFOUND με στόχο την απομόνωση και τη μελέτη της χρωματίνης που επιδιορθώνεται, μέσω του μηχανισμού εκτομής νουκλεοτιδίων (NER). Σύζευξη της μεθόδου αυτής με ανάλυση φασματομετρίας μάζας κατέληξαν σε έναν κατάλογο πρωτεϊνών, οι οποίες ενδέχεται να διαδραματίζουν κάποιο ρόλο στο δίκτυο UV-DDR. Σε αυτή τη μελέτη, χαρακτηρίστηκαν μερικές από τις πρόσφατα ευρεθείσες πρωτεΐνες. Για το σκοπό αυτό, επελέγησαν οι στρατηγικές σίγασης γονιδίων είτε μέσω της χρήσης siRNAs είτε μέσω των shRNAs, ώστε να μειωθούν τα επίπεδα των υποψήφιων DDR πρωτεϊνών, που εμπλέκονται στο μηχανισμό απόκρισης στις βλάβες του DNA. Επιπλέον, ινοβλάστες άγριου τύπου εκτέθηκαν σε υπεριώδη ακτινοβολία και, στη συνέχεια, ακολούθησε ανάλυση ανοσοφθορισμού για να επαληθευτεί η επιστράτευση των πρωτεϊνών σε σημεία τοπικής UV βλάβης (LUDs), παρέχοντας έτσι πληροφορίες για τη συμμετοχή τους στο δίκτυο UV-DDR.

Introduction

DNA Damage Response (DDR) Network

The DNA in our cells accumulates thousands of lesions and it has been estimated that each human cell is subjected to 70,000 lesions per day (*Lindahl and Barnes*, 2000), (*Ciccia and Elledge*, 2010). A sophisticated network of **DNA damage response** system has evolved to safeguard genomic integrity, as damage events occur every day in our cells. Upon sensing damage, DNA damage response can cause cell cycle checkpoint activation, transcriptional program activation, repair pathways and in case that the level of the lesion is severe it may also lead to apoptosis**.** Posttranslational modifications (PTMs) of chromatin and chromatin-associated proteins orchestrate the recruitment of key DDR players at the sites that undergo repair. Phosphorylation, ubiquitylation, SUMOylation, poly (ADP-ribosyl)ation, acetylation and methylation are among the DNA damage-induced PTMs. **Phosphorylation of histone variant H2A.X** (γH2A.X) is the most abundant chromatin modification associated with the DDR, attracting repair factors *(*Paull TT *et al., 2000).* Even though, γH2AX was demonstrated as a marker of DNA double strand breaks *(*Rogakou *et al. 1998),* Marti et al. in 2006 demonstrated that γH2A.X also appears upon NER. Melanomas have been shown to express γH2AX as a marker of ongoing or persistent DNA damage (Gorgoulis *et al. 2005*; Wasco *et al. 2008*; Nikolaishvilli-Feinberg *et al. 2013*). Many studies demonstrate that defects in specific DNA damage response (DDR) pathways are increasingly relevant in tumor development. *(*Campbell B.B *et al. 2017), (*Riaz N. *et al., 2017), (*Knijnenburg T.A *et al., 2018).* Moreover, there are chemotherapies exploiting these defects in order to target cancer cells in a selective manner. *(O'Connor M.J., 2015).* Deeper understanding of NER-DDR network may help the fight against cancer through the development of new chemotherapeutic drugs.

DNA Damaging agents

Exogenous agents, such as X-rays, ultraviolet (UV) light and various chemicals can cause genetic changes that promote cancer (*Friedberg, 2008*). Moreover, endogenous sources of DNA damage include hydrolysis, oxidation, alkylation, errors during DNA replication and mismatch of DNA bases. Both endogenous and exogenous insults can damage the genomic DNA and in case of improper repair, damages can lead to genomic instability, apoptosis, or senescence affecting the organism's development and ageing process. In order to maintain the integrity of the genome, cells have evolved a variety of repair mechanisms: mismatch repair (MMR), base excision repair (BER), **nucleotide excision repair** (**NER**), non-homologous end-joining (NHEJ), and homologous recombination (HR).

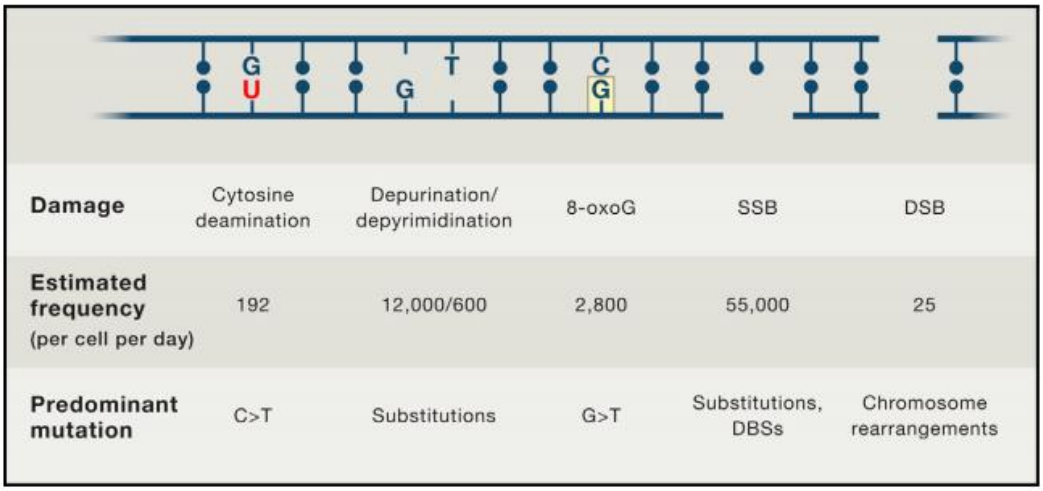

Damage	Cytosine deamination	Depurination/ depyrimidination	8-oxoG	SSB	DSB
Estimated frequency (per cell per day)	192	12,000/600	2,800	55,000	25
Predominant mutation	C>T	Substitutions	G>T	Substitutions, DBSs	Chromosome rearrangements

Figure 1: Frequencies of DNA Lesions and Mutations Associated with Dysfunctional DNA Repair.

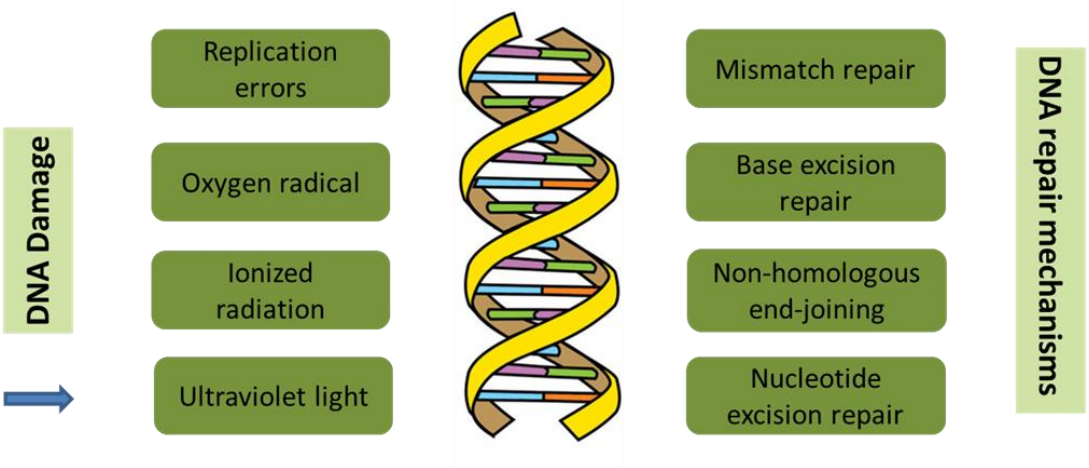

***Figure 2*:** DNA damage and DNA repair mechanisms. On the left there are presented the DNA damaging agents, while on the right there are the DNA repair mechanisms responsible for the removal of the lesions.

Nucleotide Excision Repair (NER)

Ultraviolet light is a DNA-damaging agent that induces photolesions, mainly helix-distorting cyclobutane pyrimidine dimers (**CPDs**) and pyrimidine-(6,4)-pyrimidone products (**6-4PP**), which are removed by **Nucleotide Excision Repair**. NER is critically important in the repair of UV-induced DNA lesions and is also responsible for the removal of bulky DNA adducts induced by environmental mutagens and certain chemotherapeutic agents. It can be categorized into two sub-pathways: **global genome NER** (GG-NER or GGR) and **transcription-coupled NER** (TC-NER or TCR). GG-NER repairs damages throughout the whole genome, while TC-NER is responsible for the accelerated repair of lesions in the **transcribed strand of active genes**. The two sub-pathways differ in the initial steps of DNA damage recognition whereas they share the same process for lesion incision, repair, and ligation. TC-NER is activated by the blocked RNA polymerase II complex at the lesions, while in GG-NER damage is recognized by the XPC-RAD23B or UV-DDB1/2 complex (*Fousteri and Mullenders, 2008*). Briefly, once the damage is recognized, a ~30 nucleotide single-stranded DNA segment that contains the lesion is removed by endonucleases, while the undamaged single-stranded DNA remains. DNA polymerases use it as a template to synthesize a short complementary fragment, during **unscheduled DNA synthesis**. In the final step, ligation is carried out by DNA ligase.

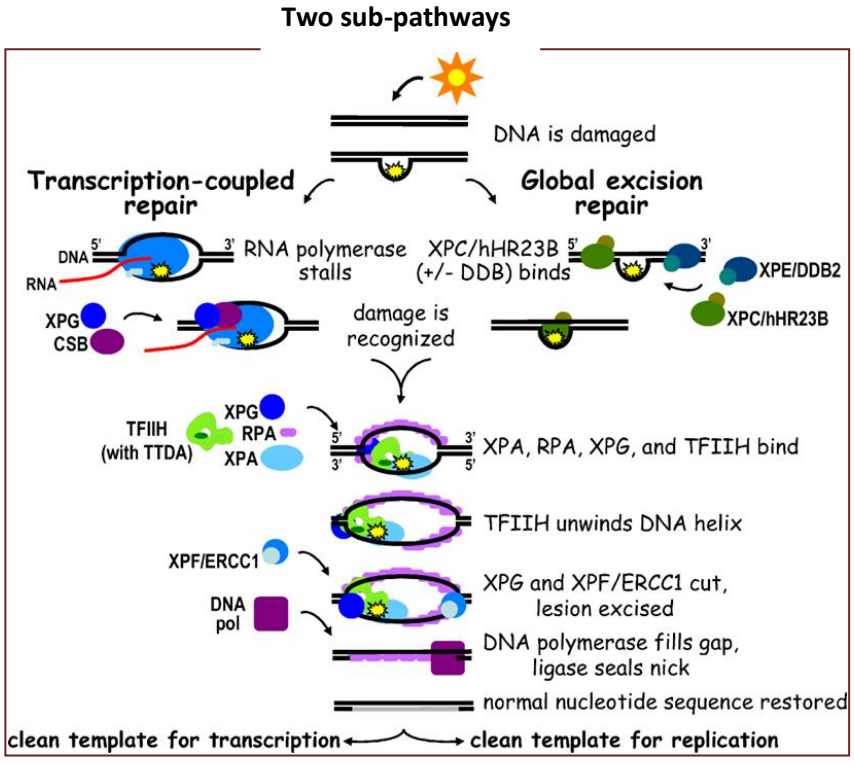

Figure 3: *Diagram of TC-NER and GG-NER sub-pathways.*

NER associated syndromes

The importance of NER mechanism is demonstrated in certain human syndromes that are characterized as defective in nucleotide excision repair processes. The clinical effects of the unrepaired DNA damage are described in the following syndromes.

GG-NER syndrome

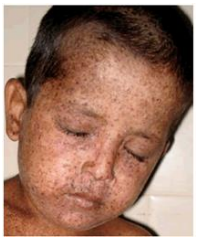

Xeroderma pigmentosum (**XP**) is a recessive genetic disorder caused by mutations in any of the 7 XP genes (XP-A to -G) as well as XP-Variant (encoding for translesion DNA polymerase eta, **Pol η**). In most XP subtypes, there is elevated risk of developing cell carcinomas on sun-exposed areas, as UV irradiation-induced DNA photoproducts are not removed by NER (Cleaver *et al. 2009*).

TC-NER syndromes

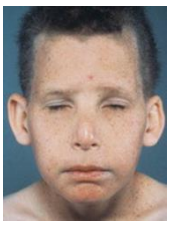

Trichothiodystrophy (**TTD**) is an autosomal recessive inherited disorder characterized by brittle hair and intellectual impairment and half of all patients have photosensitivity. Mutations in TTDN1, XPB, XPD and TTD are recognized as causing the TTD phenotype.

Cockayne syndrome (**CS**) is an autosomal recessive neurodegenerative disorder characterized by growth failure, impaired development of the nervous system, photosensitivity, eye disorders and premature aging. Mutations in the ERCC8 (CSA) or the ERCC6 (CSB) gene are the cause of CS (Bender M *et al. 2003)*.

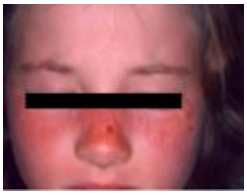

UV sensitivity syndrome (**UVSS**) is an autosomal recessive disorder caused by mutations in the ERCC6 (CSB), the ERCC8 (CSA), or the UVSSA gene. UVSS patients share some clinical features with the CS patients, but they lack the severe growth and neurological abnormalities characterizing CS patients.

State-of the-art

Accelerated native isolation of factors on unscheduled nascent DNA (aniFOUND)

The NER pathway has been reconstituted in vitro and has been extensively studied. Even though there has been a lot of effort in the field, important details of the different levels that coordinate UV-DDR network are still missing. UV-DDR needs to be further studied for better understanding of this network. Elucidating the pathways and the crosstalk between them is of great importance. In this basis, a novel antibody-free method has been developed in the laboratory of Dr. Fousteri (Stefos, Szantai *et al,. 2019, unpublished*), for the study of the UV-triggered DDR. Concisely, wild type fibroblasts were UV-C irradiated and the repaired chromatin was EdU labeled, taking advantage the unscheduled DNA synthesis, during the NER. The repaired chromatin is isolated and analyzed by Mass Spectrometry.

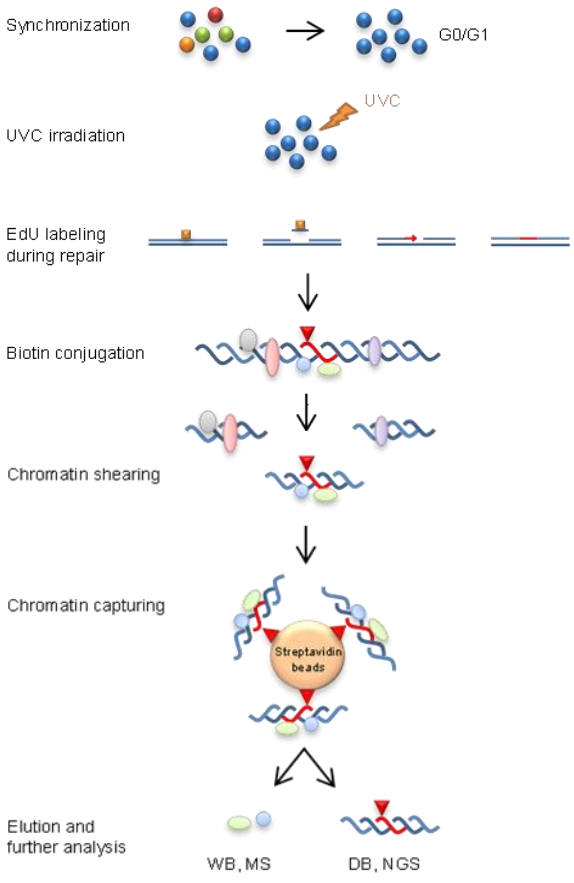

***Figure 4*:** Schematic representation of aniFOUND.

The aniFOUND-MS resulted in a list of 298 proteins, bound on the newly repaired chromatin. These UVC-induced DDR candidate proteins that have been arisen need to be validated and further characterized. Knocking down the expression of the most promising candidate proteins in 1BR.3 wild type dermal fibroblasts will highlight their implication in DDR network.

siRNAs and shRNAs as tools for gene silencing

The use of RNA interference (RNAi) is a powerful tool for the study of gene function in mammalian cells. The mechanism of RNAi is based on the sequence-specific degradation of mRNA through the cytoplasmic delivery of double-stranded RNA (dsRNA) identical to the target sequence. The applications of RNAi can be mediated through two types of molecules; the chemically synthesized double-stranded small interfering RNA (**siRNA**) or vector-based short hairpin RNA (**shRNA**). Both of them are commonly used as tools for protein knockdown. Exogenously introduced siRNA and shRNA have to be processed by endogenous microRNA (miRNA) machinery in order to be functional.

Small interfering RNAs (siRNAs) are double-stranded RNA molecules, 20-25 nucleotides in length. The Dicer enzyme catalyzes production of siRNAs from long dsRNAs (Nishina K *et al,. 2008,* Bernstein E *et al,. 2001*). siRNAs are bound by RISC and strands are separated. The antisense single-stranded siRNA component guides and aligns the RISC complex on the target mRNA and through the action of catalytic RISC protein, mRNA is cleaved (*Song JJ et al,. 2004,* Liu J *et al,. 2004*). Thus, when transfected into cells, siRNAs inhibit the target mRNAs transiently until they are also degraded within the cell.

Besides siRNA transfection, the degradation of a target mRNA, can also be induced by shRNAs. In this case, expression of shRNA in cells is accomplished by delivery of plasmids or through viral or bacterial vectors. Small hairpin RNAs (shRNA) are sequences of RNA, typically about 80 base pairs in length, that include a region of internal hybridization that creates a hairpin structure. shRNA is transcribed in the host nucleus and is processed by Drosha. The resulting pre-shRNA is then processed by Dicer and loaded into the RNA-induced silencing complex (RISC). The antisense strand directs RISC to mRNA that has a complementary sequence and represses translation of the mRNA. As a result, the shRNA leads to target gene silencing. (Paddison PJ *et al., 2002*). The benefit of shRNA is that they can be incorporated into plasmid vectors and integrated into genomic DNA for longer-term or stable expression, and thus longer knockdown of the target mRNA.

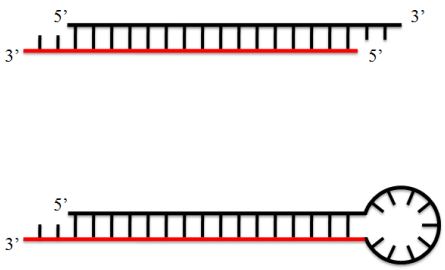

Figure 5: Structure of siRNA and shRNA. (A) siRNAs are short RNA duplexes with characteristic 3' overhangs. (B) shRNAs consist of sense and antisense sequences separated by a loop sequence.

Previously verified candidate proteins upon local UV irradiation

aniFOUND-MS resulted in a list of proteins that resided on newly repaired DNA and the presence of some proteins at the sites of repair was experimentally validated. The recruitment of Mitochondrial Calcium Uptake 2 **MICU2** (also known as EFHA1) and Testis Expressed 10 **(TEX10)** proteins were verified at the sites of UVC-induced photolesions. Based on literature, MICU1 and MICU2 are the main regulators of the mitochondrial Ca2 +-uniporter (MCU) (*Maria Patron et al., 2014*), but their precise functional role is still not clarified. **MICU2** behaves as a **pure inhibitor of MCU at low cytosolic [Ca2 +] ([Ca2 +]c**), while **knockdown of MICU2 induces** only a persistent **increase in mitochondrial Ca2 + uptake** (Jessica Matesanz-Isabel *et al., 2016*)**.** An unexpected linkage between the MICU2 and stress responses was uncovered, indicating the cardiovascular homeostasis dependence on MICU2. As it was shown in the study of Alexander G *et al., 2017*, naive *Micu2*$^{-/-}$ mice had abnormalities of cardiac relaxation, modest blood pressure elevation and developed abdominal aortic aneurysms with spontaneous rupture.

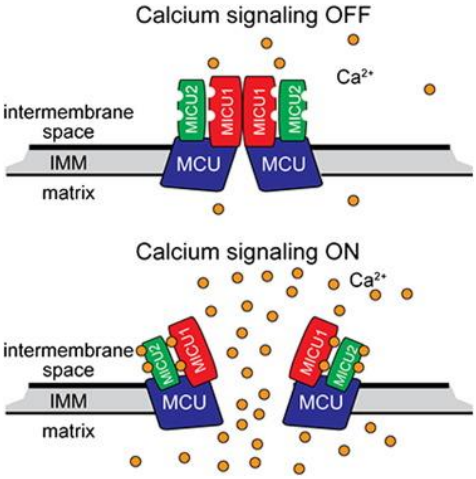

As far as the other protein is concerned, **Testis expressed 10 (TEX10),** it functions as a component of the Five Friends of Methylated CHTOP (5FMC) complex along with PELP1, WDR18, SENP3 and LAS1L (*Fanis P., 2012*). TEX10 is involved in the **nucleolar steps of 28S rRNA maturation** and the subsequent nucleoplasmic transit of the **pre-60S ribosomal subunit** (*Finkbeiner E,. 2011*). In the recent study of Xiaocong Xiang *et al., 2018*, Tex10 was found dramatically **up-regulated in human HCC tissues**, compared to normal liver tissues. Moreover, Tex10 expression was significantly up-regulated in poorly-differentiated HCC tissues and the highly metastatic HCC cell line, suggesting its potential role in HCC metastasis. Moreover, it was reported that ***Tex10* knockdown** significantly **increased drug sensitivity** of HCC **to sorafenib and cisplatin**, suggesting a possible role of Tex10 in the treatment of HCC drug resistance. In addition, it was also confirmed that Tex10 regulates CSC properties in HCC through STAT3 signaling.

Strategy-Aim

Since the above-mentioned proteins **have not been previously reported for being implicated in the UV-DDR network**, they captured our attention to investigate their role. For this purpose, siRNA transfection and shRNA lentiviral transduction were performed to knockdown them and to reveal their implication in the UVC-DDR repair network by further tests (UV sensitivity assay, colony formation assay).

At this point it is important to note that Mass Spectrometry identified four members of the 5FMC complex. **LAS1L, PELP1 and SENP3** were previously tested for their recruitment at the sites undergoing repair, but immunofluorescence results did not confirm the presence of these proteins at LUDs. As a number of technical reasons might be responsible for that, we decided to also choose one more member of this complex, LAS1L, for the knockdown experiments.

In parallel, we aimed to test and verify the recruitment of additional candidate proteins that were obtained from the aniFOUND method. **In this study**, normal human 1BR.3 fibroblasts and XP-A cells (that lack both NER sub-pathways) were locally irradiated with UV-C with the dose of 100 J/m^2 and tested by immunofluorescence staining to confirm the recruitment of candidate proteins at local UV damage sites.

Materials and Methods

Immunocytochemistry

Cell culture and irradiation

Normal htert immortalized human dermal fibroblasts (1BR.3, VH10) and NER-deficient XP-A fibroblasts were maintained under standard conditions in DMEM, supplemented with 10 % Fetal Bovine Serum and 100 units/ml of penicillin/streptomycin (Gibco) at 37°C in a 5 % CO_2 humidified incubator. Cells were grown on sterile coverslips and once 80–90% confluency was reached they were locally irradiated with 100 J/m^2 UV-C, through a 5 μm pore polycarbonate membrane filter (Merck, cat. no. TMTP04700, TETP04700). Then, they were incubated either for 1 or 4 hour to recover in 0.5% serum containing medium, together with 10 mM hydroxyurea (HU) that arrests DNA replication.

Fixing

After the indicated recovery periods, coverslips were washed with cold PBS and after an optional treatment of cytoskeleton (CSK) buffer for 5 min (to remove soluble nuclear proteins) cells were fixed immediately, using either methanol or 4% paraformaldehyde, for 10 minutes. In case of paraformaldehyde fixing, cells were permeabilized with 0.5 %Triton-X for 10 min. In both cases, cells were blocked in 10 % FBS (Sigma-Aldrich, cat. no. A9647) for 20 min at RT. In the case of anti-CPD co-staining (CosmoBio, cat. no. NMDND001), before blocking there was an extra step including the incubation of 37°C 0.1 N HCl for 10 minutes, followed by two PBS washes.

Antibody staining-Microscopy

For antibody staining, cells were incubated with the appropriate concentration of the primary antibody overnight at 4°C and were co-stained either with anti-γH2AX (Abcam, cat. no. ab22551 and ab2893) or with anti-XPG (Novus NB100-74611) or anti-CPD (CosmoBio NMDND001). The following day, cells were washed three times with wash buffer for 5 minutes and incubated for 1 hr at RT with the secondary antibodies. Cells were then washed two times with wash buffer, stained for 5 min with DAPI (1ug/ml) and washed twice again, before mounting with Mowiol (Fluka, 81381. polyvinyl alcohol 4-88). Fluorescent images were acquired with a LEICA DM2000 microscope equipped with the DFC345 FX camera and pseudocolour was applied using the LAS V4.12 software. Imaging conditions, i.e. exposure time, brightness and contrast remained identical between different conditions.

In the table below, the tested primary and secondary antibodies are listed.

REAGENT	SOURCE	IDENTIFIER
Primary Antibodies		
Mouse monoclonal **anti-ADAR1**	Santa Cruz	sc-73408
Rabbit polyclonal **anti-CCDC11**	Abcam	ab 84324
Monoclonal **anti-CPD**	CosmoBio	NMDND001
Mouse monoclonal **anti-DEK**	Santa Cruz	sc-136222
Rabbit polyclonal **ERCC2 (anti-XPD)**	GeneTex	GTX105357
Rabbit polyclonal **anti-Exo1**	Sigma-Aldrich	SAB4503568
Mouse monoclonal **anti-ELAVL1**	Santa Cruz	sc-5261
Mouse monoclonal **anti-Fbxo28**	Santa Cruz	sc-376851
Mouse monoclonal **anti-γH2A.X**	Abcam	ab22551 ab2893
Mouse monoclonal **anti-HIV-1 Tat-SF1**	Santa Cruz	sc-514351
Mouse monoclonal **anti-HNRNPA2B1**	Santa Cruz	sc-32316
Mouse monoclonal **anti-HNRNPC**	Santa Cruz	sc-32308
Goat polyclonal **anti-HNRNPH1H2**	Santa Cruz	sc-10042
Mouse monoclonal **anti-HNRNPK**	Santa Cruz	sc-32307
Mouse monoclonal **anti-HNRNPL**	Santa Cruz	sc-32317
Mouse monoclonal **anti-HNRNPM**	Santa Cruz	sc-20002
Goat polyclonal **anti-HNRNPU**	Santa Cruz	sc-13663
Rabbit polyclonal **anti-LAS1L**	Sigma-Aldrich	AV34629
Mouse monoclonal **anti-NIPBL**	Santa Cruz	sc-374625
Mouse monoclonal **anti-PELP1**	Santa Cruz	sc-390599
Mouse monoclonal **anti-PHF6**	Santa Cruz	sc-365237
Mouse monoclonal **anti-PHF21A**	Santa Cruz	sc-376844
Mouse monoclonal **anti-POLK**	Abnova	H00051426
Rabbit monoclonal **anti-RSF1**	Abcam	ab109002
Mouse monoclonal **anti-SAFB**	Abcam	ab8060
Rabbit polyclonal **anti-SFPQ**	Santa Cruz	sc-28730
Mouse monoclonal **anti-SRSF1**	Santa Cruz	sc-33652
Mouse monoclonal **anti-THOC1**	Santa Cruz	sc-514123
Mouse monoclonal **anti-TPR**	Santa Cruz	sc-271565
Mouse monoclonal **anti-UBF**	Santa Cruz	sc-13125
Rabbit polyclonal **anti-XPG**	Novus Biologicals	NB100-74611
Rabbit polyclonal **anti-ZMYND11**	Thermo Fisher	PA5-27899
Mouse monoclonal **anti-ZNF326**	Santa Cruz	sc-390606
Mouse monoclonal **anti-ZNF512**	Santa Cruz	sc-398142
Secondary antibodies		
Anti-Goat IgG H&L Alexa Fluor® 555	Abcam	ab150130
Anti-Rabbit IgG H&L Alexa Fluor® 594	Abcam	ab150080
Anti-Rabbit IgG H&L Alexa Fluor® 488	Abcam	ab150077
Anti-Mouse IgG H&L Alexa Fluor® 594	Abcam	ab150116
Anti-Mouse IgG H&L Alexa Fluor® 488	Abcam	ab150113

siRNA transfection

For the experimental purposes, wild type human fibroblasts were plated in a 6-well plate, in 4 mL DMEM growth medium with 10% (v/v) Fetal Bovine Serum (FBS) and 1% (v/v) Penicillin/Streptomycin mix. At the time of the transfection, cells were 60-70% confluent. Lipofectamine™ RNAiMAX Transfection Reagent and siRNA were both diluted in DMEM, mixed in 1:1 ratio and incubated for 5 minutes. DMEM growth medium on cells was reduced to 2 mL, the siRNA-lipid complex was added to plated cells and then, they were incubated at 37°C in a 5% CO2 incubator, for 72 hours, until they were ready to assay for gene knockdown. For the *MICU2* knock down, fibroblasts were treated with siRNA at the concentrations of 10, 5, 3 and 1 nM, while for the *LAS1L* gene knock down cells were treated with siRNA at the concentrations of 10, 2 and 1 nM. A non-targeting siRNA was used as a negative control for the knock down experiments. **The following siRNA sequences were used**:

MICU2 13.2 siRNA sequence:

5’ UUUGUUUUAUCCUUCCAGAAAGCAUAU 3’

3’ AAACAAAAUAGGAAGGUCUUUCGUA 5’

MICU2 13.3 siRNA sequence:

5’ GAAAUUAGCCCUUUAUCGCCAAGGUCU 3’

3’ CTUUAAUCGGGAAAUAGCGGUUCCA 5’

LAS1L. 13.1 siRNA sequence:

5’ CUGUGAUGUCAUCAACAACAAUGUUCU 3’

3’ GACACUACAGUAGUUGUUGUUACAA 5’

LAS1L. 13.2 siRNA sequence:

5’ CUCUCUGAGAUAAGAUUCACAAACCUG 3’

3’GAGAGACUCUAUUCUAAGUGUUUGG 5’

All controls and samples were cultured simultaneously, so as to obtain reliable results and to establish the mRNA and protein expression levels of the samples. **hs.Ri.MICU2.13 and hs.Ri.LAS1L.13 were obtained** from TriFECTa® RNAi Kit from IDT (Intagrated DNA Technologies).

RNA Extraction, cDNA Synthesis and qPCR

72 hours post-transfection, cells were collected separately for **i) RNA extraction** and **ii) protein extraction**. For the RNA extraction, growth medium was removed and 400μl of TRIzol™ Reagent was added to each well. Cells were collected and incubated for 5 minutes at RT. RNA extraction was performed using chloroform followed by isopropanol precipitation. The quality of RNA was assessed using samples of 1μg on a 1% denaturing agarose gel, stained with ethidium bromide (EtBr). The next step of the procedure was the cDNA synthesis from the mRNA molecules, using a mix of dNTPs, oligo (dT) primer and MMLV transcriptase, DTT and RNase out. An extra sample without reverse transcriptase was used to test for any genomic contamination. A water bath followed for 50 minutes, at 42°C. Once cDNAs were synthesized, quantitative PCR was performed by using 2xqPCRBIO SyGreen Mix, (containing dNTPs, $MgSO_4$, DNA polymerase and buffer), forward and reverse primer 10μM and 1:4 diluted cDNA. The expression level of the tested gene was normalized to the expression level of the GAPDH gene. In addition, a no template control (NTC) was used, as well as the no reverse transcriptase control (NRT). All qPCR reactions were performed in duplicates and Cq values were averaged.

qPCR primers for MICU2

MICU2_f1: GTC AGA CTA GCG GAG TTT AAG

MICU2_r1: GAC ATT CAT CAC CAT CCA AAT C

qPCR primers for LAS1L

Las1L_f1: CCC AAC TCC TTC GGA TCA T

Las1L_r1: CTG GGT ATA AAT GGA ACA GAT GC

Las1L_f2: TGC GAT GGG ACA CAT TTC

Las1L_r2: TCT TGC ATG TTG AGG GTT C

Protein extraction and Western Blot

For protein extraction, cells were washed with PBS, scraped and pelleted by centrifugation. RIPA buffer without SDS was used, so as to lyse the cells and extract proteins from the fibroblasts. RIPA enables the disruption of membranes, releasing nuclear and cytoplasmic proteins. Moreover, protease inhibitors were also added to inhibit the degradation of proteins. The standard Bradford assay followed to determine the total protein concentration in the given samples. The knockdown efficiency on the protein level was determined with Western Blot analysis, loading same amount of proteins of the different samples. and normalizing to the amount of GAPDH (Ambion AM4300).

For the MICU2 and LAS1L proteins, the anti-MICU2 (ab101465) and the anti-LAS1L (AV34629, Sigma) primary polyclonal rabbit antibodies were used, at 1:500 and 1:800 dilutions, respectively. A common goat anti-Rabbit IRDye 680RD secondary antibody was used (LI-COR Biosciences 926-68071), at 1:10000 dilution.

Irradiation of knock down cells-UV survival assay

Wild type and knockdown fibroblasts were plated and cultured for 48 hours after transfection in 100-mm Petri dish **at a density of $1x10^6$**. Cells were then exposed to UV-C light and their cell viability was determined. Briefly, medium was removed, cells were washed with 1X PBS and were subjected to UV at the doses of 0 J/m^2, 5 J/m^2 and 10 J/m^2. Fresh medium was added afterwards and 24 hours post irradiation, cells were trypsinised. Trypan Blue dye was used to determine the number of viable cells. For the experimental purposes the MICU2_siRNA#3 (IDT hs.Ri.MICU2.13.3) and the LAS1L siRNA#2 (IDT hs.Ri.LAS1L.13.2) duplexes were used since these gave the best knock-down efficiency. A non-targeting siRNA duplex provided by the TriFECTa DsiRNA Kit (IDT) was used as control. Non-viable cells are turning blue, while viable cells remain unstained. Cells were counted under the microscope, using Neubauer chamber.

Colony formation

For the colony formation assay, 500 fibroblasts were seeded in 60mm plates. *MICU2* siRNA#3 in the concentration of 5nM (since it gave the best knockdown efficacy results), untransfected wild type fibroblasts and the non-targeting siRNA control were seeded in p60 plates, were UV-C irradiated at the doses of 0 J/m^2, 5 J/m^2 and 10 J/m^2 and incubated at 37°C in 5% CO2 conditions, as controls. Colony formation was allowed to proceed for 14 days. Cells were then washed with 1 ml of PBS (Invitrogen), stained with Coomassie Brilliant Blue G-250 Dye (20279) for 15 min, and finally washed three times with 1 ml of double distilled H2O.

shRNA lentiviral transduction

Cloning of Tet-pLKO-puro

The Tet-pLKO-Puro plasmid (Addgene #21915) was digested with EcoRI and AgeI restriction enzymes sequentially and the vector was purified by agarose gel electrophoresis. To generate shRNA-expressing plasmids, the stuffer DNA was replaced with the annealed shRNA oligonucleotides that were inserted between the 2 cloning sites of the vector. Previously, for the annealing the oligo powders were dissolved in ddH2O to 0.1nmol/μl and were mixed with 10X annealing buffer. Mixtures were placed in a 95°C water bath and cooled down naturally to RT (2-3 hours). Finally, the 1:400 diluted annealed oligos and the cut vector were mixed in a standard ligation reaction. 2 shRNA constructs targeting *MICU2* and 2 shRNA constructs targeting *TEX10* mRNAs were generated together with the Tet-pLKO-scramble-shRNA plasmid was that was used as negative control.

MICU2 13.2 shRNA sequence

MICU2 sh_2 sense:

5’**CCGG**TTTGTTTTATCCTTCCAGAAAGCATAT**CTCGAG**ATATGCTTTCTGGAAGGATAAAACAAA**TTTTT**-3’

MICU2 sh_2 anti-sense:

5’**AATTAAAAA**TTTGTTTTATCCTTCCAGAAAGCATAT**CTCGAG**ATATGCTTTCTGGAAGGATAAAACAAA-3’

MICU2 13.3 shRNA sequence

MICU2 sh_3 sense:

5’**CCGG**GAAATTAGCCCTTTATCGCCAAGGTCT**CTCGAG**AGACCTTGGCGATAAAGGGCTAATTTC**TTTTT**- 3’

MICU2 sh_3 anti-sense:

5’**AATTAAAAA**GAAATTAGCCCTTTATCGCCAAGGTCT**CTCGAG**AGACCTTGGCGATAAAGGGCTAATTTC- 3’

Tex10 shRNA #2 sequence

Tex10 sh_2 sense:

5’-**CCGGG**CAGCAAGTTCTTAATATT**CTCGAG**AATATTAAGAACTTGCTGC**TTTTT**-3’

Tex10 sh_2 anti-sense:

5’-**AATTAAAAA**GCAGCAAGTTCTTAATATT**CTCGAG**AATATTAAGAACTTGCTGC-3’

Tex10 shRNA #3 sequence

Tex10 sh_3 sense:

5’-**CCGG**AGCTACTGCCCTCCGAATTTA**CTCGAG**TAAATTCGGAGGGCAGTAGCT**TTTTT**-3’

Tex10 sh_3 anti-sense:

5’-**AATTAAAAA**AGCTACTGCCCTCCGAATTTA**CTCGAG**TAAATTCGGAGGGCAGTAGCT-3’

Scrambled shRNA sequence

SCR sh_sense:

5’-**CCGG**GTACAGCCGCCTCAATTCT**CTCGAG**AGAATTGAGGCGGCTGTAC**TTTTT**-3’

SCR sh_anti-sense:

5’-**AATTAAAAA**GTACAGCCGCCTCAATTCT**CTCGAG**AGAATTGAGGCGGCTGTAC-3’

The sequential restriction digestions are described in the following tables:

Reagents	µl
Tet-pLKO-Puro 5 µg	1.2
10X buffer CutSmart	10
AgeI	2
WFI	86.8
Total volume	**100**

Reagents	µl
Eluted purified plasmid DNA	60
10X buffer NEB 1.1	10
EcoRI	3
WFI	27
Total volume	**100**

DH5α competent cells were transformed with the resulted constructs and cells were plated on LB agar plates with 100 µg/ml ampicillin and incubated at 37 °C overnight. The following day, isolated colonies were picked, inoculated into 5 ml Terrific Broth (TB) with ampicillin and were incubated in a 37 °C shaker overnight. The NucleoSpin Plasmid Kit (Macherey-Nagel 740588.50S) was used for the isolation of plasmid DNA and *Sla*I digestion was used to confirm the insertion of the double stranded sh oligos. Positive clones were sent for sequencing to confirm the presence of the correct insert.

HEK Cell Culture, transfection and transduction

4 million Lenti 293T cells were seeded in collagen-coated p10 dishes. Tet-pLKO-shRNA transfer plasmid, psPAX2 packaging plasmid and pMD2.G envelope plasmids were mixed in 2.8:2:1 ratio. A GFP gene containing pLL.3 plasmid was used for monitoring the transfection efficiency. 4-6 h post-transfection, fresh normal medium was added. Lenti 293T cells were returned to 37 °C for 72 h to produce viral particles. Media containing the viruses were collected, cleaned from cell particles by a 0.45 µM filter and stored at -80°C.

For transduction $2x10^5$ 1BR.3 human fibroblasts were seeded with 8µg/ml polybrene in 6-well plate in a volume of 2 ml to which 1 ml viral supernatant was added. 4 hr later, shRNA expression was triggered upon the addition of doxycycline (1µg/ml). The following day fresh medium was added to the cells with doxycycline.

RNA Extraction, cDNA Synthesis and qPCR

For the RNA extraction, the cDNA synthesis and the qPCR the same procedure was followed, as it is described in the siRNA transfection methods. In case knock-down efficiency was checked, total RNA was extracted 72 hours upon doxycycline induction. When the expression of the sh oligo was monitored, RNA was collected on the second day after transduction.

For the cDNA synthesis with the stem-loop primers, 3.5µl 10µM stem-loop primer against scrambled sh oligo were used, 1.4µl 360ng/µl oligo dT, 0.4µl 25mM dNTP mix, 6.7µl RNA/water mix containing 1µg RNA (for 1 sample). An incubation step was followed at 37°C.

qPCR primers for Text10

Tex10_f1:

5’-TGTTGACCAATGCGATCTTG-3’

Tex10_r1:

5’-CCTGAACACTTCCACTCTTCAAT-3’

Stem loop Human Scrambled primer for the cDNA synthesis

5’-GTCGTATCCAGTGCAGGGTCCGAGGTATTCGCACTGGATACGACAGAATT-3’

Forward human Scrambled primer for the qPCR

5’-CACGCAGTACAGCCGCCT-3’

Reverse human Scrambled primer for the qPCR

5’-CCAGTGCAGGGTCCGAGGTA-3’

Results

Identification and validation of new UVC-induced DDR players

Some of the novel DDR candidate proteins that were obtained from the aniFOUND-MS were tested by immunofluorescence staining to determine which of them are recruited to sites that undergo NER. Wild type fibroblasts and XP-A cells were exposed to local UV-C irradiation at a dose of 100J/m^2 and left for 1hr recovery in low serum containing media, in the presence of Hydroxyurea. Staining with an antibody against XPG, the human endonuclease that cuts 3' to DNA lesions during NER, was used as a control of the UV-C LUD sites. Among the proteins listed in table 1, the presence of Nipped-B-like protein (**NIPBL**) was verified at XPG-labeled DNA damage sites in wild type (VH10) cells (*Fig 6a*), while no NIPBL protein was detected at the LUDs in NER-deficient XPA cells (*Fig 6b*). For the NIPBL detection (green), the damage sites were XPG-labeled (red) and nuclei were DAPI-**stained** (blue). In figure 6, it is shown the recruitment of the cohesin loader protein **NIPBL** to sites that undergo repair only in wild type fibroblasts, indicating that **NIPBL recruitment at UV-C damaged chromatin depends on functional NER mechanism.**

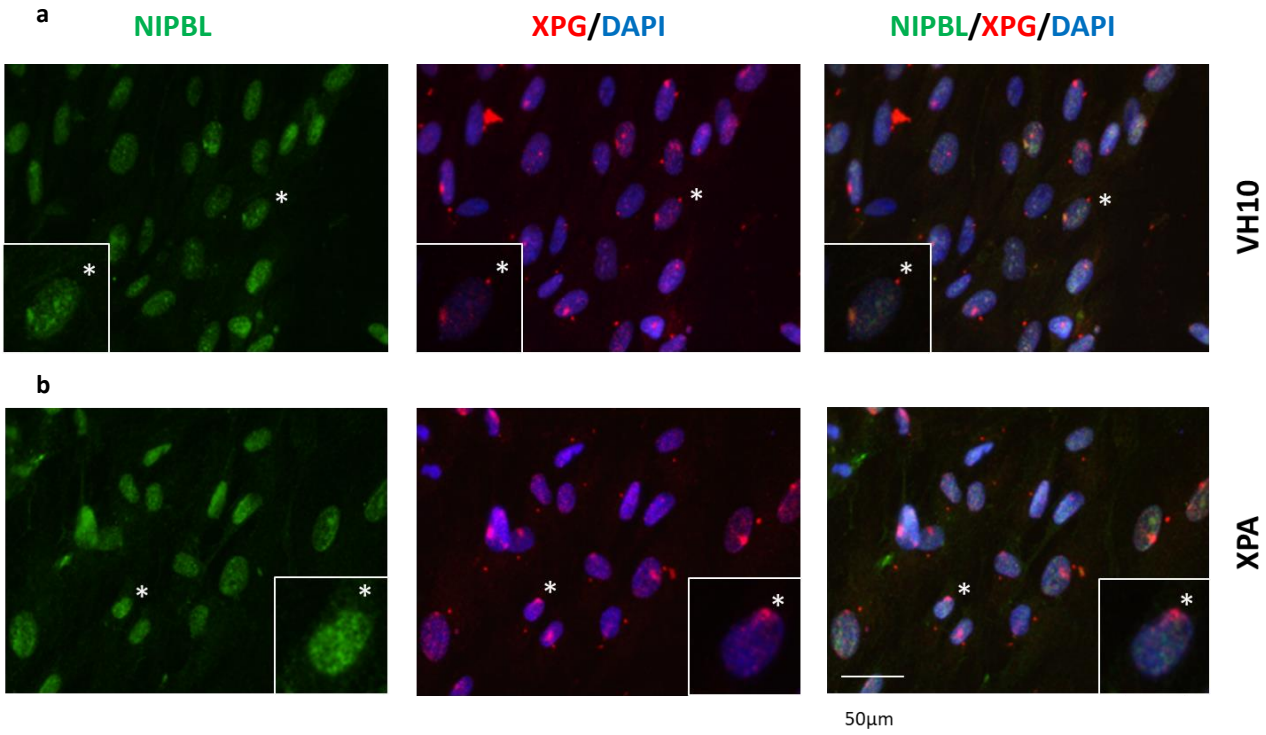

Figure 6: NIBPL and XPG staining in VH10 and XPA cells. Wild type human fibroblasts and XPA cells were exposed to 100 $J/m^2$of UV, through 5µm-pore-size filters, left for 1hr to recover and were immunolabeled with antibodies (a) (upper panel) NIPBL co-localization with XPG signal in wild type fibroblasts. (b) In NER-deficient cells, NIBPL is not present at the LUDs (lower panel) Scale bar = 50 µm.

The second protein that was validated for its recruitment at the UV-induced damage sites was **RSF1** (Remodelling and Spacing Factor 1). In this experiment, the damage sites were labeled with antibodies against CPD (red) and RSF1 (green). RSF1 was detected at CPD-labeled sites in wild type cells (*Fig 7a*) but not in XPA cells (*Fig 7b*). The fact that RSF1 is present at the LUDs only in wild type fibroblasts demonstrates that **its recruitment is also NER dependent.**

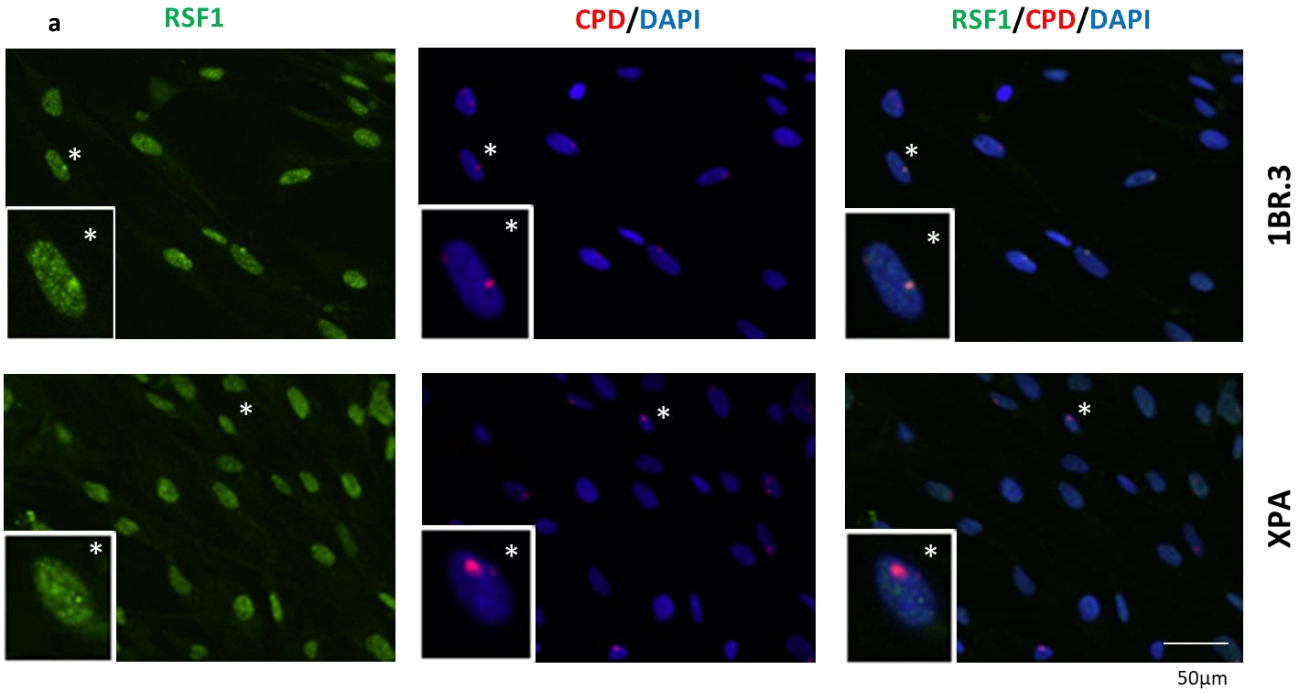

Figure 7: RSF1 and CPD staining in 1BR.3 and XPA cells. Human fibroblasts and XPA cells were exposed to 100 $J/m^2$of UV, through 5µm-pore-size filters, left for 1hr to recover and were immunolabeled with antibodies (a) (upper panel) RSF1 co-localization with CPD signal in wild type fibroblasts. (b) (lower panel) In NER-deficient cells, RSF1 is not recruited at the LUDs. Scale bar = 50 µm.

Knockdown of MICU2 and LAS1L in human fibroblasts

Mitochondrial Calcium Uptake 2 **MICU2** (or also known as EF-hand domain family member A1 isoform 1: EFHA1) was previously verified to be recruited in the nucleus at the UV-induced damage sites that undergo repair, after 4 hours of recovery by Dr. Eszter Szantai (Dr. Fousteri's lab). In the mitochondrium MICU2 acts as Ca2+ sensor and gatekeeper of the Mitochondrial Calcium Uniporter (MCU), preventing calcium uptake under resting conditions.

With the Mass Spectrometry analysis of the proteins pulled-down with the aniFOUND method, 4 out of 5 members of the **5FMC complex** was found (TEX10, LAS1L, PELP1 and WDR18). The recruitment of **TEX10** could also be verified by immunofluorescence technique.

Since neither MICU2, nor the 5FMC complex have ever been reported to have a role in the UV-DDR network, a protein knockdown strategy was designed to study their implication. Our

first approach was using the siRNA transfection methodology to knockdown MICU2 and LAS1 Like Ribosome Biogenesis Factor protein (LAS1L). The latter one is a nucleolar protein required for cell proliferation and ribosome biogenesis.

***MICU2* Knockdown**

3nM and 5nM siRNA concentration-mRNA expression levels

The procedure followed included siRNA transfection of cells, isolation of total RNA, cDNA synthesis and qPCR reactions, using *MICU2* and *GAPDH* specific primers. The purpose of all the above is to assess the relative knockdown efficiency of a set of 3 siRNA duplexes. For the *MICU2* gene knock down, fibroblasts were treated with siRNA at the concentrations of 10, 5, 3 and 1 nM. (Results are shown only for the two best siRNA duplexes and for the two best concentrations.)

In the following diagrams, the relative mRNA expression levels are represented (% of non-targeting control-NTC), in siRNA#2 and siRNA#3 sets, after the **siRNA transfection at the concentration of 3 and of 5nM**.

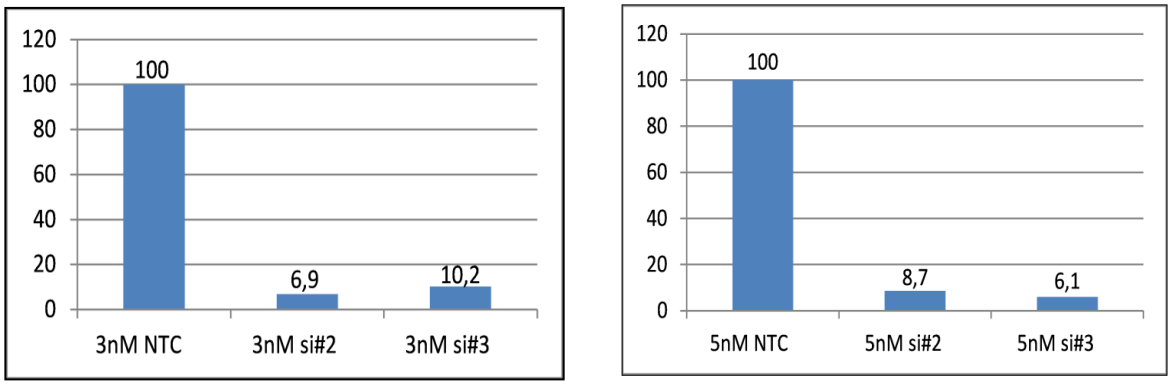

***Figure 8*:** Relative *MICU2* mRNA expression levels with siRNA#2 and siRNA#3 duplexes, after siRNA transfection at the concentration of 3nM (left) and of 5nM (right).

In the siRNA transfection at the concentration of 3nM, the mRNA expression level of *MICU2* with siRNA #2 and #3 is 6.9% and 10.2%, respectively. In the siRNA transfection at the concentration of 5nM, the mRNA expression level of *MICU2* with siRNA #2 and #3 is 8.7% and 6.1%, respectively.

3nM and 5nM siRNA concentration- protein expression levels

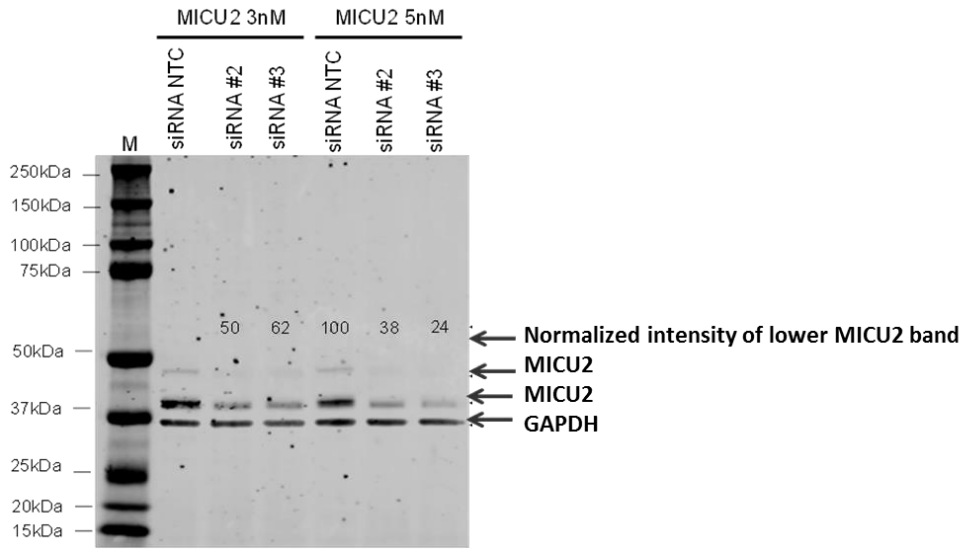

Figure 9: Western blot analysis, monitoring the amount of MICU2 protein, after transfection of siRNA at the concentration of 3 and 5nM.

Based on the Western blot results, two bands were revealed, a more abundant ~40 kDa and a less abundant ~48 kDa size band. Both of them are supposed to be MICU2 specific, since the relative intensity of the bands decreases or fully disappears, upon knock-down. In the siRNA transfection at the concentration of 3nM, the relevant amount of MICU2 protein (lower band) decreases from 100% (NTC) to 50% (siRNA#2) and to 62% (siRNA#3). In the siRNA transfection at the concentration of 5nM, the relevant amount of MICU2 protein decreases from 100% (NTC) to 38% (siRNA#2) and to 24% (siRNA#3). In conclusion, **MICU2 siRNA #3 at the concentration of 5nM showed the best knock down efficacy.**

***LAS1L* Knockdown**

1nM and 2nM siRNA concentration-mRNA expression levels

For the *LAS1L* gene knock down, fibroblasts were treated with 3 siRNA duplexes at the concentrations of 10, 2 and 1 nM. Results are shown only for the two best siRNA duplexes and for the two best concentrations.

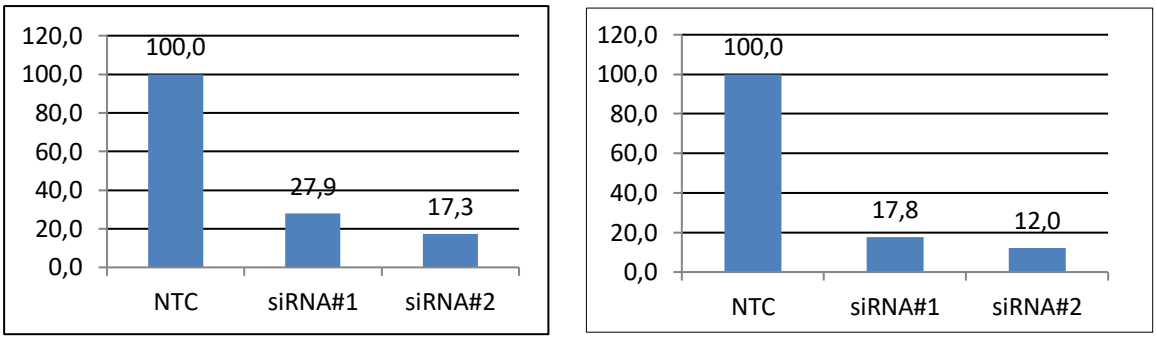

***Figure 10*:** Relative *LAS1L* mRNA expression levels with siRNA#1 and siRNA#2 duplexes, after siRNA transfection at the concentration of 1nM (left) and of 2nM (right).

With the siRNA transfection at the concentration of 1nM, qPCR results showed 72,1% knock down efficiency of *LAS1L* gene using siRNA#1 and 82.7% knock down efficiency using siRNA#2. With the siRNA transfection at the concentration of 2nM, results showed 82.2% knock down efficiency of LAS1L gene using siRNA#1 and 88% knock down efficiency, using siRNA#2. **To conclude, siRNA#2 at the concentration of 2nM presents the highest knock down efficacy of LAS1L gene.**

1nM and 2nM siRNA concentration- protein levels

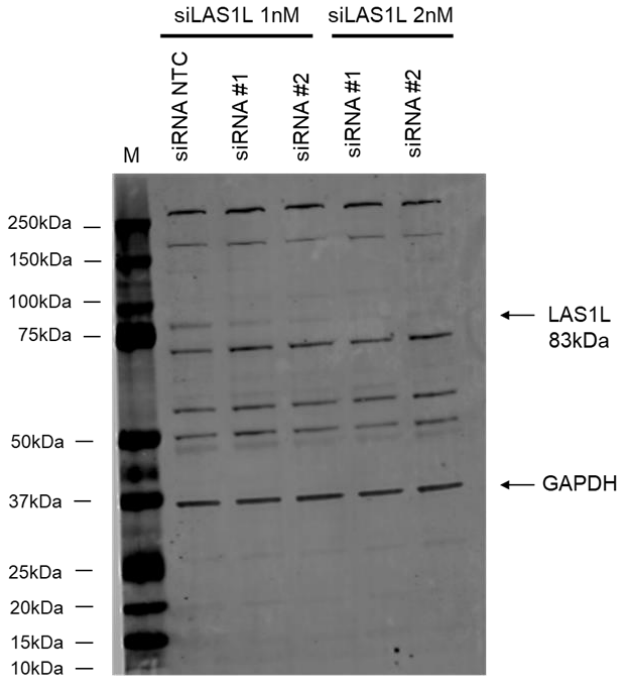

The immunoblot analysis, revealed a ~83 kDa band, corresponding to LAS1L protein, while there were also higher and lower molecular weight bands detected, corresponding to non-specific bands. According to the results, in the siRNA transfection at the concentration of 2nM, the relevant amount of LAS1L protein decreases from 100% (NTC) to ~0% (siRNA#2). **In conclusion, the siRNA#2 in the concentration of 2nM showed the best efficacy**.

Figure 11: Western blot analysis monitoring the relevant amount of LAS1L protein, after the siRNA transfection, at the concentration of 1 and 2nM.

Irradiation of knock down cells-UV survival assay

In the following procedure, untransfected fibroblasts, the non-targeting siRNA control, the *MICU2* siRNA#3 in the concentration of 5nM, the non-targeting control siRNA and *LAS1L* siRNA#2 at the concentration of 3nM were used, since they gave the best knockdown efficacy results. 50000 cells per 6 wells were seeded and siRNA transfected 1BR.3 cells were UV-C irradiated at the doses of 0 J/m^2, 5 J/m^2 and 10 J/m^2. The table below shows the number of live cells, according to the different conditions.

Joules/m²	NTC	*MICU2* si#3
0	160000	182500
5	107500	85000
10	175000	125000

Joules/m²	NTC	*LAS1L* si#2
0	192500	112500
5	97500	80000
10	140000	115000

Table 2: Number of live cells/well upon UV-C irradiation at the doses of 0 J/m^2, 5 J/m^2 or 10 J/m^2.

J/m2	NTC	MICU2 #3
0	100	100
5	67,2	46,6
10	109,3	68,5

J/m2	NTC	LAS1L#2
0	100	100
5	50,6	71,1
10	72,7	102,2

Table 3: Percentage of live cells/well upon UV-C irradiation at the doses of 0 J/m^2, 5 J/m^2 or 10 J/m^2 in comparison with the number of the non-targeting control cells.

It is very important to note that -due to technical problems during counting, the numbers in the 5 J/m^2conditions - should not be taken into consideration, just like cell number in the 10 J/m^2 condition of NTC in the MICU2 experiment. Based on our results, measurements of survival rate of the knockdown cells in response to UV exposure were not conclusive. Therefore, a colony formation assay using MICU2 knock-down fibroblasts was carried out.

Colony formation assay

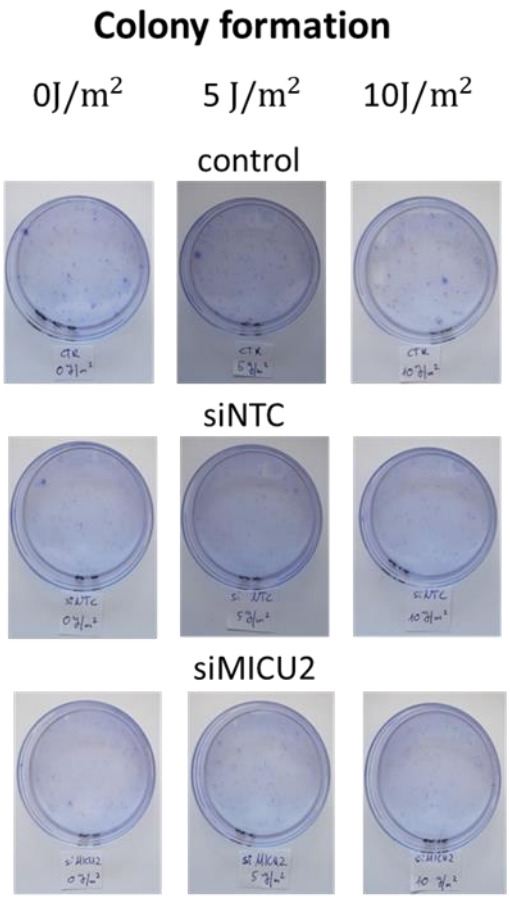

For the experimental purposes, 500 fibroblasts were seeded in 60mm plates. Untransfected fibroblasts, fibroblasts transfected with non-targeting siRNA construct and *MICU2* siRNA #2 were tested for their ability to form colonies upon UV irradiation at the doses of 0 J/m^2, 5 J/m^2 and 10 J/m^2. Fourteen to twenty-five days after UV irradiation, the colonies were stained and analyzed for the number of cells and size. The results with colonies were based on two independent experiments.

Unfortunately, this experiment was also non conclusive, as no colony formation with more than 20 cells was detected also in the si non-targeting control cells (control plate) either.

Figure 12: Colony formation assay. Cells (n = 500) were plated in 60mm plates, in DMEM medium containing 10% (v/v) FBS. Cells were cultured for 14-25 days at 37 °C, stained with **Coomassie Blue** dye and counted.

MICU2 and TEX10 knockdown by shRNA transduction of human fibroblasts

The siRNA transfection experiments were successful, however the UV survival and the colony formation assays were non informative, regarding the effects of knocking down *MICU2* and *LAS1L* DDR candidate genes. For the following experiments, lentiviral shRNA transduction of human fibroblasts was performed, as a cost-effective strategy. The Tet-pLKO-Puro (also known as pLKO-Tet-On) plasmid was chosen to transfer specific shRNA sequences for *MICU2*

and this time *TEX10* mRNAs. As a negative control, a scrambled shRNA sequence that does not target any human mRNA was used. The plasmid vector has a total size of 10.634 base pairs, a cloning site between the *AgeI* and the *EcoRI* restriction sites and has also the TetR element and a puromycin resistance gene. The inserted sh oligos are under the expression of H1/TO promoter. The double digestion with *EcoRI* and *AgeI* produces bands at ~8kb and 1.8kb, matching the backbone and stuffer, respectively.

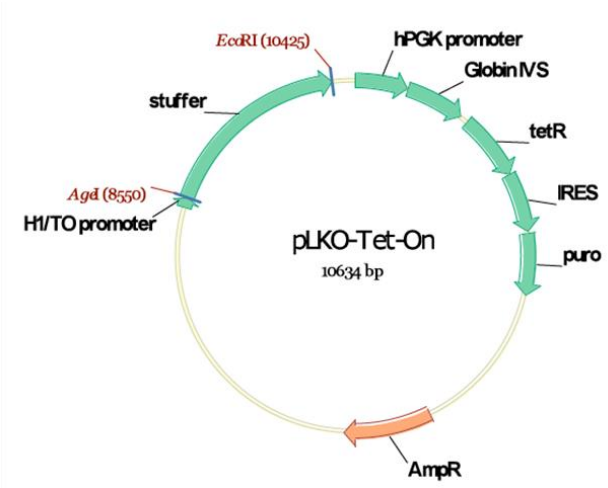

Figure 13: Plasmid map of the vector, highlighting the 2 cloning sites, the TetR element and the puromycin resistance gene.

The vector was digested with *AgeI* and *EcoRI* sequentially and gel purified. For the cloning, the sh oligos were annealed and ligated with the digested plasmid, in a regular ligation reaction.

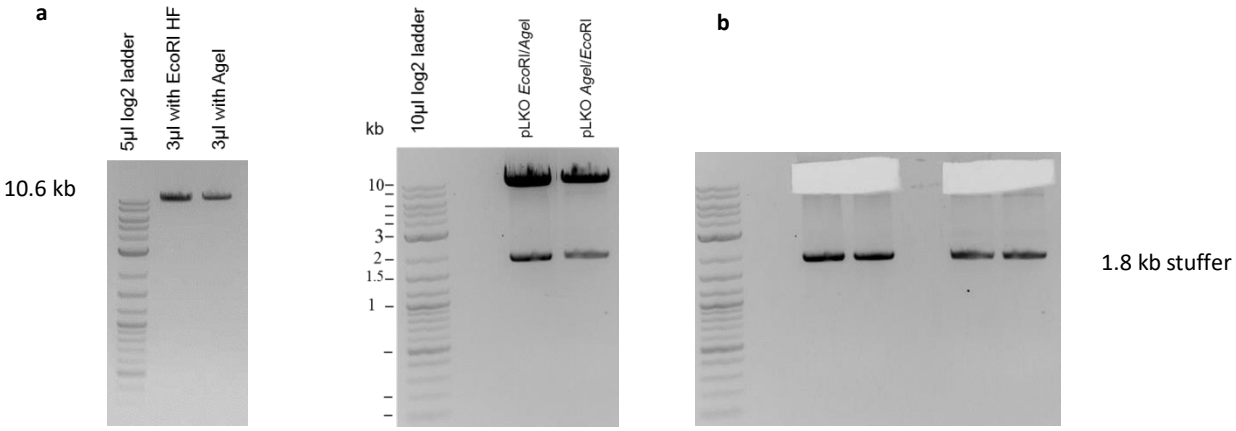

Figure 14: (a) Digestion of Tet-pLKO-Puro with AgeI and EcoRI enzymes. The expected fragment size is 10633bp. (b) Gel Purification and isolation of the upper DNA band.

The generated constructs that express scramble shRNA, shRNA targeting *MICU2* and *TEX10* mRNAs are under the expression of **H1/TO promoter**. In the following figure, the modified plasmid maps of the generated constructs are presented.

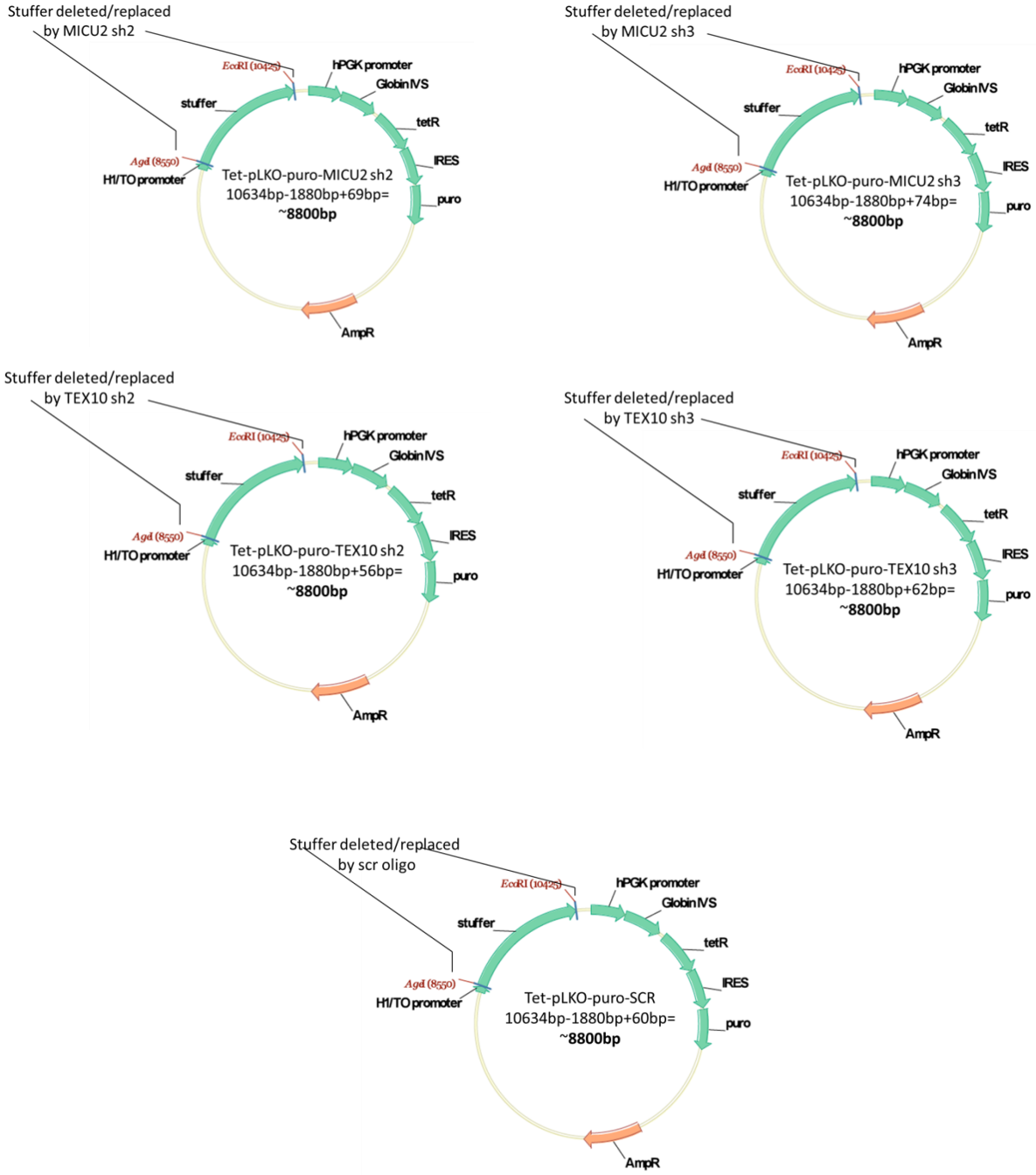

Figure 15: Plasmid maps of modified pLKO vectors. 2-2 shRNA-expressing plasmids targeting *MICU2* and *TEX10* mRNAs and a negative control vector, containing scrambled shRNA that does not target to any human mRNA.

Transformation, isolation and digestion of plasmid DNA

The generated constructs were used to transform *DH5α* competent cells. Single colonies were isolated and grown overnight at 37°C, and the following day plasmid purification was carried out. The constructs were verified by enzyme digestion, using the *XhoI* **(SlaI) restriction enzyme** that recognizes C^TCGAG site and cuts in the shRNA inserts and in the backbone of the plasmid. The three expected fragment sizes are ~8.4kbp, 190bp and ~140bp. In the following figure, the described procedure is represented. In order to confirm the identity of the inserts a sequencing step was followed (data not shown).

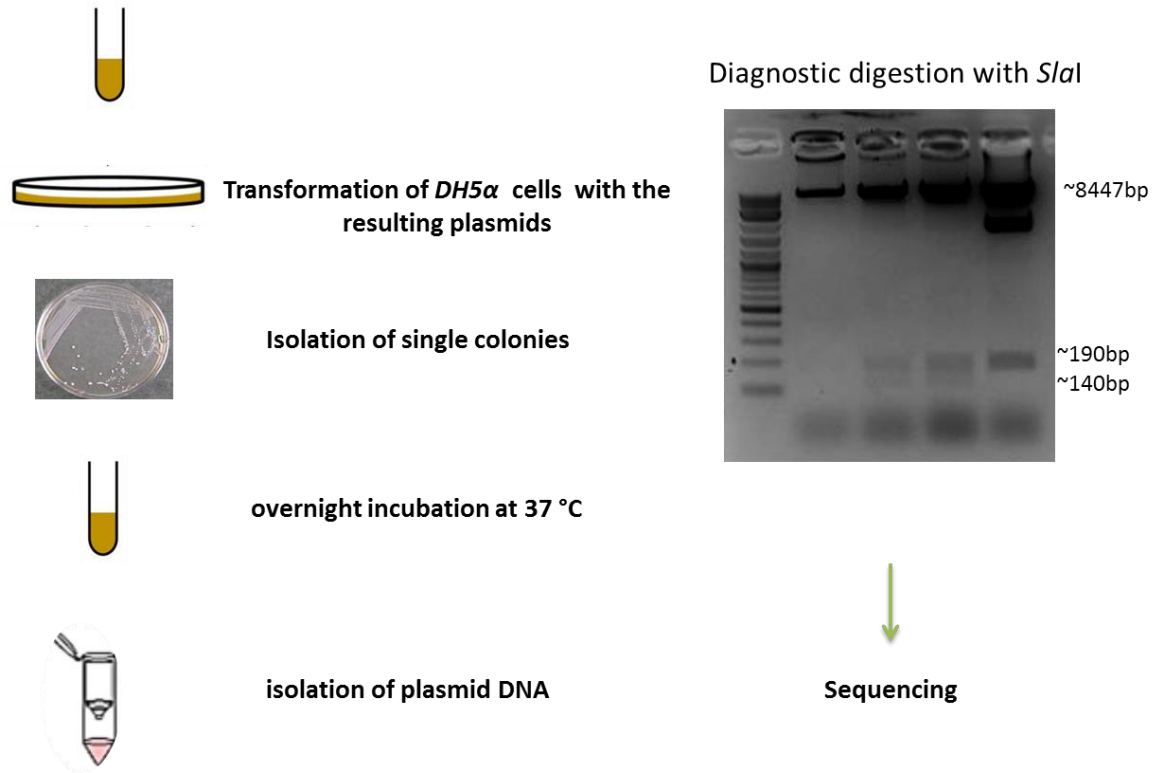

Figure 16: Transformation, isolation and digestion of plasmid DNA. The diagnostic digestion was performed using the *XhoI* **restriction enzyme** that cuts in the middle of the sh oligo inserts. The three expected fragment sizes are ~8.4kbp, 190bp and ~140bp.

Generation of lentiviral shRNAs for knocked-down cell lines

The next step of the procedure was the transfection of adherent Lenti-X 293T cells, using a three-plasmid combination: Tet-pLKO-puro transfer vectors and the lentivirus envelope and packaging plasmid mix of pMD2.G and PsPAX2. A non-inducible GFP expressing pLL.3 vector was used as a positive control to monitor the transfection efficiency. 1 BR.3 fibroblasts were transduced with the harvested viral supernatant. The following day sh oligo expression was induced by adding doxycycline in a final concentration of 1µg/mL. Upon induction, tetR is removed from the tet-operator sequences (tetO) inserted into the promoter, allowing transcription of shRNA and leading to RNAi-mediated knockdown of the targeted genes. In the following figure, the procedure of lentiviral sh oligo delivery is outlined and the transduced cells are depicted in 6-well plates in the presence/absence of doxycycline.

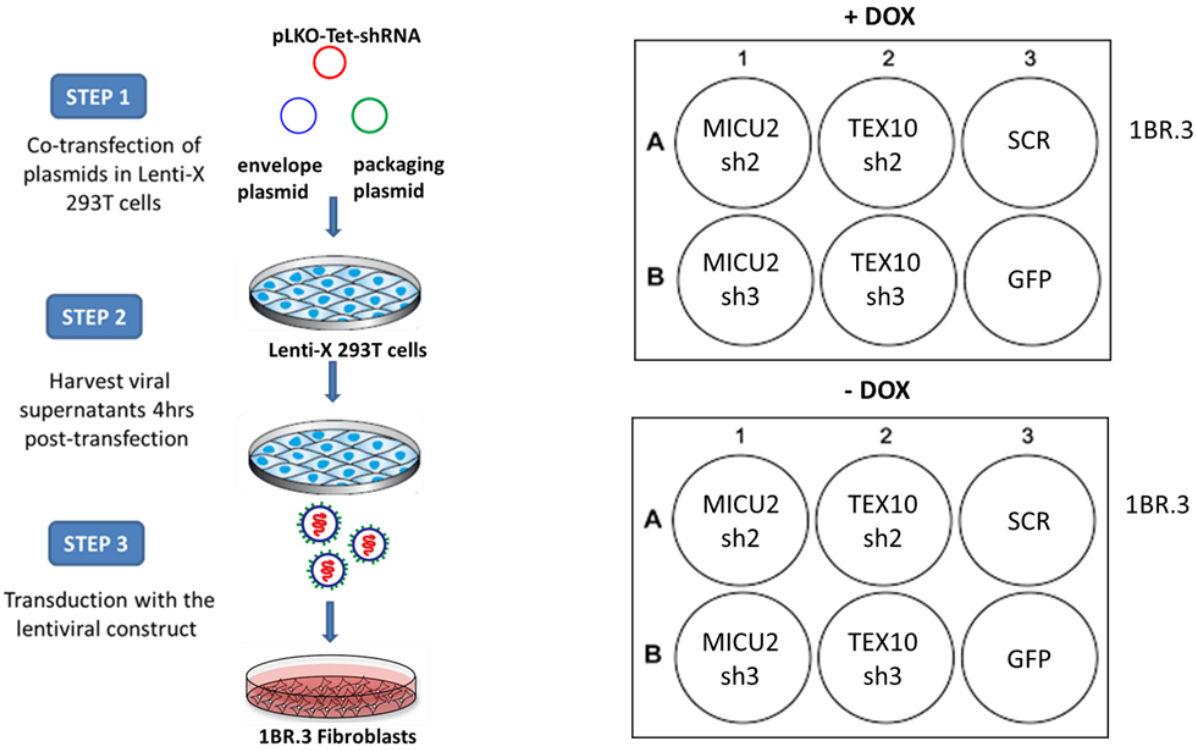

.

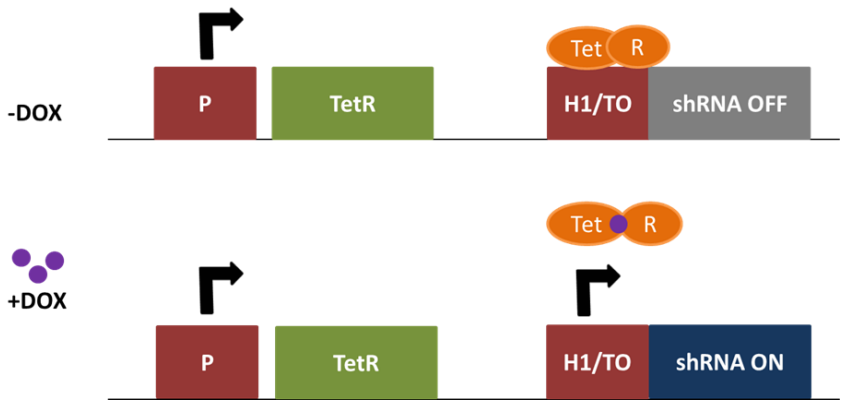

***Figure 17*: (a)** Schematic outline of the co-transfection of Lenti-X 293T transfer vector, encoding shRNAs against *MICU2* and *TEX10* mRNAs. Once lentiviral constructs are generated, they are used to transduce human fibroblasts **(b)** Culture of fibroblasts in the presence of doxycycline (+) compared to fibroblasts in the absence of doxycycline (-) (**c**). Doxycycline inducible lentiviral system.

After transduction of fibroblasts with the lentiviral constructs and treatment with doxycycline, total RNA was extracted and the mRNA was converted into complementary DNA (cDNA) in order to test the efficiency of the transduction. First, RNA samples were tested for genomic contamination and degradation.

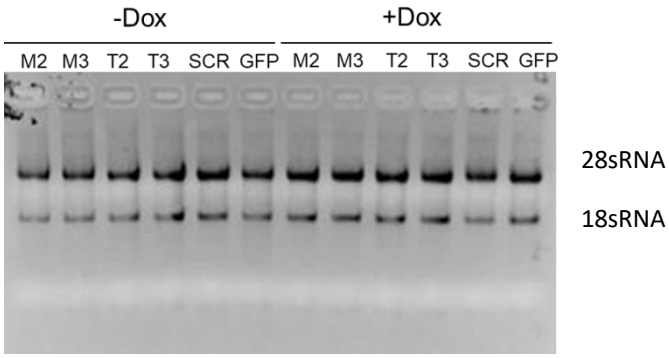

Figure 18: RNA analysis by agarose gel electrophoresis. The 28S and 18S RNA bands are indicated.

RNA integrity was assessed by observing either the staining intensity of the major ribosomal RNA (rRNA) bands or a smear that refers to degradation. As can be seen in *Figure 16*, the 28S and 18S RNA bands are indicated and no or a little DNA contamination is visible.

Next, qPCR was performed to monitor the mRNA levels of the targeted genes and scrambled oligo expression level. In case of testing the scrambled sh oligo expression, during cDNA synthesis stem-loop primers specific for the scrambled sh oligo were used as well together with the oligo dT primers. Data obtained from qPCR analyses of mRNA levels demonstrated **low MICU2 knockdown effect** and **no expression of the scrambled oligo (**qPCR measuring *TEX10* mRNA level was not carried out yet**)**. To address this, qPCR was performed to monitor the mRNA levels of TetR, indicating transduction efficiency. Our negative control was the cDNA obtained from the cells transduced with pLL.3-GFP vector that does not contain TetR gene, while as a positive control we used cDNAs from a stable cell line that contained TetR in a much higher number than it was expected in our cells. Interestingly, **some TetR expression could be monitored**, confirming the presence of integrated lentiviral particles in some of the fibroblasts. The knock down outcome was not efficient and there was no scrambled oligo expression visible, indicating that probably only a small percentage of the fibroblasts had integrated the lentiviral constructs, implying to low transduction efficiency.

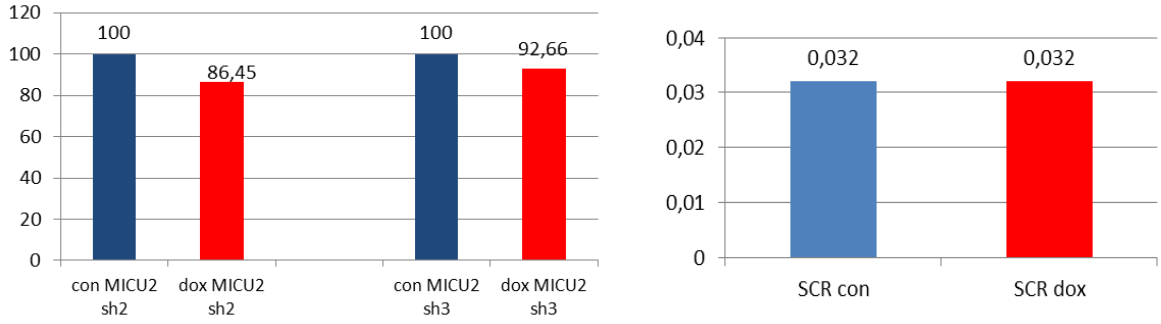

***Figure 19*:** Relative *MICU2* mRNA expression levels of fibroblasts in the absence (control) and presence of doxycycline (left). Relative scramble sh oligos expression in – and in + doxycycline conditions (right). Expression levels are normalized to GAPDH.

Since the results were not encouraging, our strategy was to select the clones that were resistant to puromycin. The basis of this concept is that, in addition to the TetR regulatory element, vectors also express the puromycin resistance gene, permitting the positive selection of transduced cells. Thus, cells were treated with 2.5 µg/ml puromycin (optimal concentration was previously defined with a kill curve experiment) and transduced colonies were isolated. Puromycin-resistant cells were transferred into 12 well plates and after reaching confluency, they were split to two 6-wells for testing KD efficiency. The following day into one of the wells doxycycline was added. 72 hours after induction, RNAs were isolated, cDNA was synthesized and qPCR was carried out. The clones showing a relative high KD efficiency were further cultured in the presence of puromycin, while negative clones were discarded.

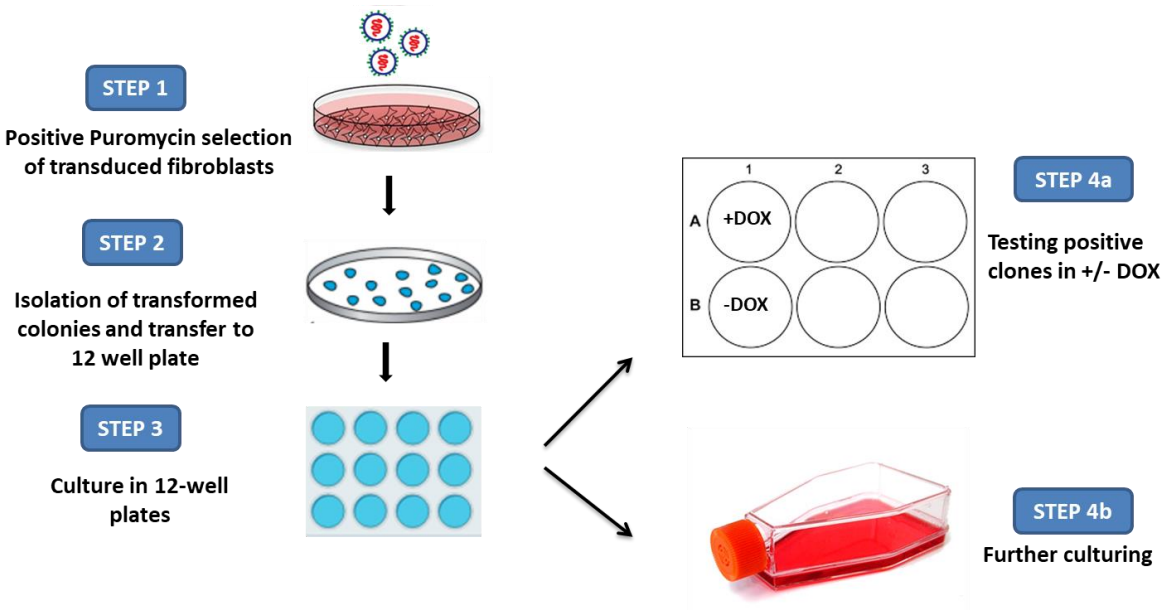

Figure 20: Flowchart of puromycin selection. Fibroblasts were treated with puromycin. Transduced clones that were pyromucin resistant were isolated, cultured and treated upon doxycycline. These clones were tested in the presence/absence of doxycycline and their transduction efficiency was monitored.

Total RNA was extracted and the mRNA was converted into complementary DNA (cDNA) in order to test the KD efficiency. Next, qPCR was performed to monitor the mRNA levels of the gene of interest. Data obtained from qPCR analyses of some of the already tested MICU2 clones are presented in the following graph.

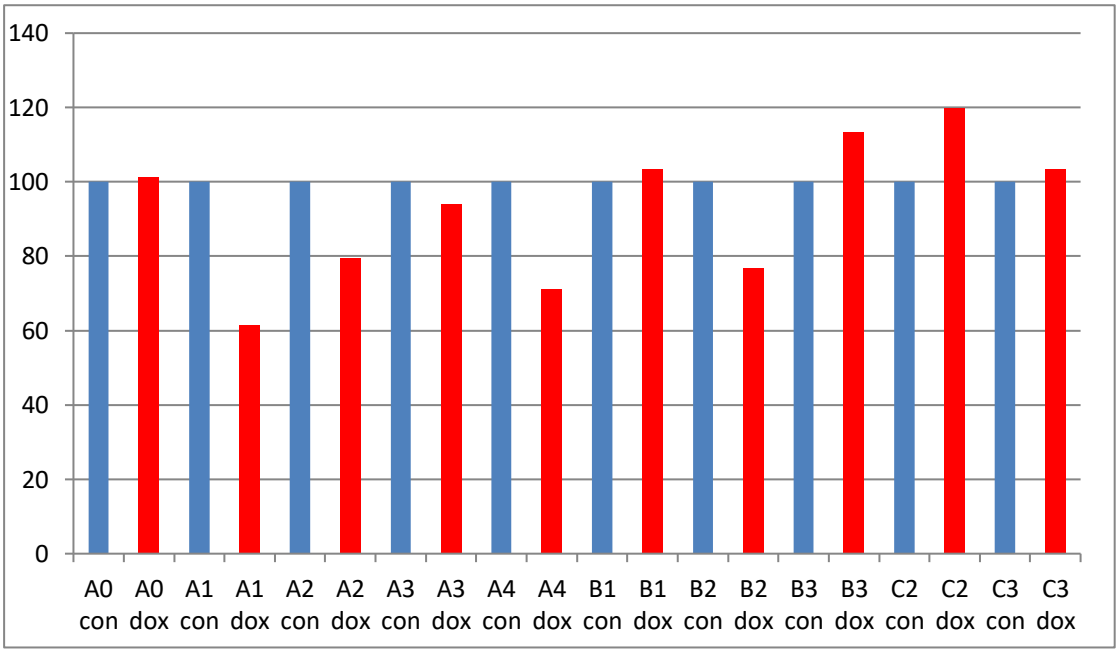

Figure 21: Expression of *MICU2* mRNA in puromycin resistant transduced fibroblasts, cultured in the absence/in the presence of doxycycline.

In the above figure, *MICU2* mRNA expression levels are depicted from the clones that have been tested so far. Blue bars represent the mRNA expression levels of puromycin resistant fibroblasts cultured in the absence of doxycycline, while red bars represent MICU2 mRNA expression levels of puromycin resistant fibroblasts, upon doxycycline treatment. In most tested clones, qPCR showed no big differences between the puromycin resistant clones, treated without and upon doxycycline. However, there are a few clones where MICU2 knockdown effect could be monitored, but not in a satisfying level.

As far as the TEX10 mRNA and the scrambled sh oligo expression levels are concerned, puromycin resistant clones are being cultured to be tested, but results are not yet available.

Discussion

In our everyday lives, we are exposed to exogenous agents such as X-rays, ultraviolet (UV) light and various chemicals that can cause genetic changes, promoting cancer. Although a large number of lesions result in single-strand DNA (ssDNA) breaks during the repair, they are also converted to the more dangerous DNA double-strand breaks (DSBs) (*Friedberg, 2008*). The DNA Damage response (**DDR**) is a crucial signaling network that safeguards genomic integrity and comprises at least 450 proteins that recognize DNA damage, initiate repair or instruct the cell to stop growing or even die (*Pearl et al., 2015*). Dysregulation of this network compromise genomic integrity in normal cells and aberrant DDR and deficient DNA repair are strongly associated with **cancer** and **aging** *(Fernandez-Capetillo 2010, Lukas et al., 2011, Mei-Ren Pan et al,. 2016).* Links between pathological aging, cancer and DNA damage/ repair are apparent and our understanding of the role of DNA repair has become much clearer. Nevertheless, a number of questions are still remaining regarding the regulation of the multilayered DDR process.

The **aniFOUND** method was developed by Dr G. Stefos and Dr E. Szantai (Dr Fousteri research team), for the isolation and characterization of the repaired chromatin, after the genotoxic stress of UV-C irradiation. This method, coupled to MS analysis, resulted in a list of proteins the presence of which on the chromatin during repair needed to be experimentally verified.

In this study, we focused on the immunofluorescence validation of the recruitment of novel DDR candidate proteins at local UV damage sites and on the generation of knockdown cell lines, to study their implication in the UV-DDR network. Human wild type (1BR.3 or VH10) and NER-deficient (XP-A) fibroblasts were locally irradiated with 100 J/m^2. The immunofluorescence based detection of the novel candidate DDR proteins confirmed the recruitment of **NIPBL and RSF1,** as well as MICU2 and TEX10, at the sites that undergo repair, upon UV-C irradiation. Based on the immunofluorescence validation, **NIPBL** protein co-localizes with XPG signal at LUDs, only in wild type fibroblasts. Previously, it has been reported that NIPBL is recruited to DNA DSBs (*Oka, 2011*). Our results demonstrate the **recruitment of NIPBL** in sites of UVC-induced damages in **wild type fibroblasts.** However, it is not recruited to lesions in XPA-deficient cells. We came to the conclusion that recruitment of NIPBL, upon UV-C irradiation, does **depend on NER mechanism and specifically on the damage excision step of NER**. The second verified protein, **RSF1**, co-localizes with CPD signal in some of the LUDs at wild type fibroblasts. The fact that **RSF1** is not recruited at LUDs in XP-A cells, highlights that its presence at the DNA damage sites is also **NER dependent.** Previous studies indicate that RSF1 is required for efficient DNA repair and is also required for the efficient repair of DSBs (*Fabio Pessina, 2014, Min et al., 2014*). Moreover, in the study of *Min, 2018* it is reported that RSF1 stability is significantly upregulated in response to DNA damage, followed by downregulation of its stability as γH2AX is induced. Even though RSF1 has been described to be implicated in DSB repair, its involvement in NER has not been reported before.

According to preliminary data and the previously verified candidate proteins at the LUDs, we aimed to generate knockdown cell lines, in order to characterize the potential role of MICU2, LAS1L and TEX10 proteins (the latter two are components of the 5FMC complex) in the UV-DDR network. Based on literature, none of these proteins are known to be involved in DDR and as far as the **MICU2 protein** is concerned, there are no reports for its nuclear role. Having this in our concern, we thought that it would be interesting to knockdown these proteins in human fibroblasts and characterize their role in the UV-DDR network. It is important to note that both **LAS1L** and **TEX10** are components of **the Five Friends of Methylated** CHTOP but **only the recruitment of TEX10 was validated at the LUDs**. Other members of the complex were also identified by the aniFOUND-MS and even though we did not manage to validate their recruitment at the LUDs, this is not evidence that these proteins are not present at the lesions.

In this basis, siRNA gene silencing was used to effectively reduce MICU2 and LAS1L protein levels in wild type fibroblasts and to study the functional consequences of their absence. First, human fibroblasts were transfected with different siRNAs targeting *MICU2* and *LAS1L* mRNAs. Based on western blot analysis, *MICU2* siRNA #3 at the concentration of 5nM showed best knock down efficacy, decreasing the protein amount to 24%. Moreover, *LA1SL* siRNA#2 at the concentration of 2nM decreased protein amount close to ~0%. Despite the successful knockdown results, UV survival and the colony formation assays were not conclusive.

To address these issues, we considered to rebuild our strategy performing **cost-effective lentivirus mediated shRNA knockdown** for **MICU2**, and this time, **TEX10** protein. We attempted to establish MICU2 and TEX10 knockdown in 1BR.3 cell lines as well as a cell line that expresses a non-targeting scrambled sh oligo. For this purpose, we used a **doxycycline inducible gene knockdown system**, to deliver sh oligo containing lentiviral particles to human fibroblasts. The Tet-On system is well characterized and has been studied extensively in the context of viral vectors. Thus, Tet-pLKO-sh oligo vectors were generated and co-transfected with envelope and packaging plasmids in Lenti-X 293 T cells, in order to produce lentiviral particles. The vectors developed in this study should be a powerful tool for doxycycline inducible RNA interference.

Since transduction efficiency seemed to be poor, puromycin selection was carried out and colonies are being cultured and constantly tested for knock-down efficiency or for scrambled sh oligo expression. Since it is still an ongoing process, out of the 13 MICU2, 11 TEX10 and 7 scrambled cell lines we show the qPCR result of the first X MICU2 cell lines. Cell lines with the biggest mRNA knock-down effect will be tested with western blot for protein levels as well. In case we end up having cell lines that upon induction show an appreciable knockdown on protein level, plethora of experiments can be carried out, including the UV survival and colony formation assays as well, to understand the role of these proteins in DDR.

Conclusions: In this study, recruitment of previously identified DDR candidate proteins - at the UV-induced damage sites was tested by immunocytochemistry. **NIBPL** and **RSF1** were found to be recruited at the sites that undergo repair, after 1 hour of recovery. In addition, **MICU2** and **TEX10** recruitment was also verified by other lab members. In particular, NIBPL and RSF1

were found to be recruited in a NER- and XPA- dependent manner, indicating that damage incision and re-synthesis of the resulting gapped DNA was required for their recruitment. Our data thus fully validate the principle of the aniFOUND methodology and reveal NIBPL and RSF1 involvement in NER-mediated synthesis of the damaged chromatin. As these proteins haven't been reported to be implicated in DDR network, we aimed to generate knockdown cell lines, using siRNA transfection and shRNA lentiviral transduction of human fibroblasts. Even though we managed to decrease the targeted protein levels using the siRNA transfection, the UV survival and the clonogenic assays were not conclusive, hence the lentiviral knockdown system was an attractive strategy to go on with. The shRNA lentiviral transduction was inefficient therefore **puromycin selection** was carried out to **create stable cell lines**. Testing mRNA and protein levels of the puromycin resistant clones upon doxycycline induction is in progress.

Future perspectives:

When the generation of stable knock-down cell lines will be successful, the following experiments will be performed for the functional characterization of MICU2 and TEX10 proteins. KD cell lines will be examined in **survival, clonogenic and transcription recovery assays** in response to UV irradiation and will be compared to NER-proficient and -deficient cell lines. The role of the candidate proteins in repair will also be monitored by quantification of the UV damage remaining in the cells-by Dotblot- in different time-points upon UV irradiation. Moreover, the genomic localization of the candidate proteins before and after UV-C irradiation will be studied using the **ChIP-seq** technique. Finally, **immuno-precipitation experiments coupled with MS, and RIP experiments** will help to identify protein-protein and RNA–protein interactions, respectively.

In the unfortunate event of not getting any efficient KD clones, further optimization needs to be carried out.

- Low efficiency of transduction is a common problem in knock down assays. To monitor the transduction efficiency, we should create a GFP expressing Tet-**pLKO-Puro plasmid. Using this as a control we could determine the transfection and transduction efficiency with flow cytometry. This could help us optimizing the experimental conditions.**
- Another suggested strategy could be **the increase of transduction efficiency by Lentiviral spinfection method.** Briefly, "Spin-fection" is achieved by plating cells into a multi-well plate along with the virus supernatant. A low speed 2 hr long spinning of the plate concentrates the virus around the cells and helps the viral integration into the target cells, thus increasing the transduction efficiency.

References

1. Repair of endogenous DNA damage. Lindahl T, Barnes DE Cold Spring Harb Symp Quant Biol*. 2000, 127-33.*

2. Transcription-coupled nucleotide excision repair in mammalian cells: molecular mechanisms and biological effects Fousteri, M., Mullenders, L.H., 2008. Cell Res. 18, 73–84

3. The DNA damage response: making it safe to play with knives. Ciccia, A., and Elledge, S.J. (2010). TMol. Cell 40, 179–204

4. Single-vector inducible lentiviral RNAi system for oncology target validation. Dmitri Wiederschain, Wee Susan, Lin Chen, Alice Loo, Guizhi Yang, Alan Huang, Yan Chen, Giordano Caponigro, Yung-mae Yao, Christoph Lengauer, William R. Sellers & John D. 2009, Cell Cycle, 8:3, 498-504, DOI: 10.4161/cc.8.3.7701

5. Comprehensive analysis of hypermutation in human cancer.Campbell B.B., Light N., Fabrizio D. Cell. 2017;171:1042–1056.e10.

6. Pan-cancer analysis of bi-allelic alterations in homologous recombination DNA repair genes. Riaz N., Blecua P., Lim R.S. Nat Commun. 2017;8:857.

7. Repair pathway choices and consequences at the double-strand break. Ceccaldi R., Rondinelli B., D'Andrea A.D. Trends Cell Biol. 2016;26:52–64.

8. The DNA damage response in immunotherapy and radiation Knijnenburg T.A., Wang L., Zimmermann M.T. Cell Rep. 2018;23:239–254.e6. Adv Radiat Oncol. 2018 Oct-Dec; 3(4): 527–533.

9. Genomic and molecular landscape of DNA damage repair deficiency across the cancer genome atlas. O'Connor M.J. Targeting the DNA damage response in cancer. Mol Cell. 2015;60:547–560.

10. A critical role for histone H2AX in recruitment of repair factors to nuclear foci after DNA damage. Paull TT, Rogakou EP, Yamazaki V, Kirchgessner CU, Gellert M, Bonner WM. Current Biology. 2000;10(15):886–895

11. H2AX phosphorylation within the G1 phase after UV irradiation depends on nucleotide excision repair and not DNA double-strand breaks. Marti TM, Hefner E, Feeney L, Natale V, Cleaver JE Proc Natl Acad Sci U S A. 2006 Jun 27; 103(26):9891-6.

12. PARP inhibitors: Synthetic lethality in the clinic. Lord CJ, Ashworth A Science. 2017 Mar 17; 355(6330):1152-1158As

13. Short hairpin RNAs (shRNAs) induce sequence-specific silencing in mammalian cells. Paddison PJ, Caudy AA, Bernstein E, Hannon GJ, Conklin DS (April 2002). Genes & Development. 16 (8): 948–58. doi:10.1101/gad.981002

14. Efficient in vivo delivery of siRNA to the liver by conjugation of alpha tocopherol. Nishina K, Unno T, Uno Y, Kubodera T, et al. Mol. Ther. 2008;16:734–740

15. Role for a bidentate ribonuclease in the initiation step of RNA interference. Bernstein E, Caudy AA, Hammond SM, Hannon GJ. Nature. 2001;409:363–366

16. Crystal structure of Argonaute and its implications for RISC slicer activity. Song JJ, Smith SK, Hannon GJ, Joshua-Tor L. Science. 2004;305:1434–1437

17. Argonaute2 is the catalytic engine of mammalian RNAi. Liu J, Carmell MA, Rivas FV, Marsden CG, et al. Science. 2004;305:1437–1441

18. Disorders of nucleotide excision repair: the genetic and molecular basis of heterogeneity. Cleaver JE, Lam ET, Revet I Nat Rev Genet. 2009 Nov; 10(11):756-68.

19. What syndrome is this? Cockayne syndrome. Bender M, Potocki L, Metry D. Pediatric Dermatology. November 2003;20(6):538-540

20. Intrauterine programming of ageing Fernandez-Capetillo O., EMBO Rep. , 2010, vol. 11 (pg. 32-36)

21. The chromatin response to DNA damage and its role in genome integrity maintenance. Lukas J, Lukas C, Bartek J., Nat Cell Biol. , 2011, vol. 13 10(pg. 1161-1169)

22. Connecting the Dots: From DNA Damage and Repair to Aging. Mei-Ren Pan, Kaiyi Li, Shiaw-Yih Lin, and Wen-Chun Hung, International Journal of Molecular Sciences. 2016 May; 17(5): 685, doi:10.3390/ijms17050685

23. The RSF1 Histone-Remodelling Factor Facilitates DNA Double-Strand Break Repair by Recruiting Centromeric and Fanconi Anaemia Proteins. Fabio Pessina, Noel F. Lowndes ‘201, 4doi.org/10.1371/journal.pbio.1001856

24. TM-dependent chromatin remodeler Rsf-1 facilitates DNA damage checkpoints and homologous recombination repair. Min S, Jo S, Lee HS, Chae S, Lee JS, Ji JH, Cho H Cell Cycle. 2014; 13(4):666-77.

25. Post-Translational Regulation of the RSF1 Chromatin Remodeler under DNA Damage. Sunwoo Min, Yong Won Choi, Hansol Yun, Sujin Jo, Jae-Hoon Ji, and Hyeseong Cho, Mol Cells. 2018 Feb 28; 41(2): 127–133 doi: 10.14348/molcells.2018.2244

26. Recruitment of the cohesin loading factor NIPBL to DNA double-strand breaks depends on MDC1, RNF168 and HP1γ in human cells. Oka Y, Suzuki K, Yamauchi M, Mitsutake N, Yamashita S Biochem Biophys Res Commun. 2011 Aug 12; 411(4):762-7

27. Independent mechanisms recruit the cohesin loader protein NIPBL to sites of DNA damage. Christopher Bot, Annika Pfeiffer, Fosco Giordano, Dharani E. Manjeera, Nico P. Dantuma, and Lena Ström, J Cell Sci. 2017 Mar 15; 130(6): 1134–1146. doi: 10.1242/jcs.197236

28. LAS1L interacts with the mammalian Rix1 complex to regulate ribosome biogenesis. Castle CD, Cassimere EK, Denicourt C. Mol Biol Cell. 2012 Feb;23(4):716-28. doi: 10.1091/mbc.E11-06-0530

29. The SUMO system controls nucleolar partitioning of a novel mammalian ribosome biogenesis complex. Finkbeiner E, Haindl M, Muller SEMBO J. 2011 Mar 16; 30(6):1067-78.

30. Proline, glutamic acid and leucine-rich protein-1 is essential for optimal p53-mediated DNA damage response. Nair BC, Krishnan SR, Sareddy GR, Mann M, Xu B, Natarajan M, Hasty P, Brann D, Tekmal RR, Vadlamudi RK Cell Death Differ. 2014 Sep; 21(9):1409-18

31. MICU1 and MICU2 Finely Tune the Mitochondrial Ca2+ Uniporter by Exerting Opposite Effects on MCU Activity Maria Patron, Vanessa Checchetto, Anna Raffaello, Enrico Teardo, Denis Vecellio Reane, Maura Mantoan, Veronica Granatiero, Ildikò Szabò, Diego De Stefani, Rosario Rizzuto Molecular Cell, March 2014, 726-737, https://doi.org/10.1016/j.molcel.2014.01.013